FRACTURE DETECTION USING AZIMUTHAL P-WAVE AMPLITUDE VARIATION WITH OFFSET (AVOA) IN A CLASTIC RESERVOIR, EASTERN CENTRAL SAUDI ARABIA

BY

Ali Hassan Al-Gawas

A Thesis Presented to the
DEANSHIP OF GRADUATE STUDIES

KING FAHD UNIVERSITY OF PETROLEUM & MINERALS

DHAHRAN, SAUDI ARABIA

In Partial Fulfillment of the
Requirements for the Degree of

MASTER OF SCIENCE

In

GEOPHYSICS

May 2015

KING FAHD UNIVERSITY OF PETROLEUM & MINERALS

DHAHRAN- 31261, SAUDI ARABIA

DEANSHIP OF GRADUATE STUDIES

This thesis, written by **Ali Hassan Al-Gawas** under the direction his thesis advisor and approved by his thesis committee, has been presented and accepted by the Dean of Graduate Studies, in partial fulfillment of the requirements for the degree of **MASTER OF SCIENCE IN GEOPHYSICS.**

Dr. Abdullatif A. Al-Shuhail
(Advisor)

Dr. Abdulaziz Al-Shaibani
Department Chairman

Dr. SanLinn Ismail Kaka
(Member)

Dr. Salam A. Zummo
Dean of Graduate Studies

Dr. Khalid Al-Ramadan
(Member)

4/2/16
Date

To my beloved mother, father, wife, kids and sisters.

ACKNOWLEDGMENTS

First, I am most thankful to ALLAH, the most gracious, for guiding me through every aspect of my life.

I would like to express my gratitude to my thesis advisor, Dr. Abdullatif Al-Shuhail, for his supervision, support and valuable guidance he has provided me. I would like to thank my committee members Dr. SanLinn Ismail Kaka and Dr. Khalid Al-Ramadan for their support and positive critiques. I thank all faculty and staff of Earth Science Department in King Fahad University of Petroleum & Minerals for their support and encouragement through my enjoyable learning experience.

Thanks to Saudi Aramco management for providing the data for this work and for giving me the permission to publish it. Special thanks for the management of the Reservoir Characterization Department, Gas Fields Characterization Division for their encouragement and support. Special thanks to Aus Al-Tawil, Mohammed Ateeq Al-Ghamdi, Hatem Al-Hendi and Marwan Al-Thagafy for their full support.

I would like to thank Brian Wallick for his support, patience, guidance while I was under his mentorship all these years. A special thank-you goes to Dr. Ismail Ozkaya, who gave me so much of his time. I could not have finished without you. Thanks to Weiqi Bai, Nicoli Garner & Ashraf Hussain, who contributed in many ways to the outcomes of this thesis. Thank you to Jan Buiting, Peter Crisi and Youness ElOuair for reviewing this thesis and providing me with their valuable feedback.

Finally yet importantly, I would like to thank my parents, wife and kids for their support, encouragement, patience and prayers through all these years.

TABLE OF CONTENTS

LIST OF TABLES

LIST OF FIGURES

ABSTRACT

Full Name : Ali Hassan Mohammed Al-Gawas

Thesis Title : Fracture Detection Using Azimuthal P-wave Amplitude Variation with Offset (AVOA) in a Clastic Reservoir, Eastern Central Saudi Arabia

Major Field : Geophysics

Date of Degree : May 2015

The late Carboniferous clastic Unayzah-C reservoir in Eastern Central Saudi Arabia is a potential deep, low porosity, possibly fractured reservoir. It is a challenge for the geoscientist to map the top and bottom of the Unayzah-C reservoir due to low signal-to-noise ratio (SNR) and limited bandwidth in the conventional 3D seismic data. A related challenge is to delineate and characterize fracture zones within the Unayzah-C reservoir. To overcome those challenges, 3D full-azimuth broadband seismic data were acquired using point receivers, low frequency sweeps down to 2 Hz, and 6-km patch geometry. The new data show significant enhancement in continuity and resolution of the reflection data, which lead to improved mapping of the top of the Unayzah-C.

Since the new dataset has rectangular patch geometry with full inline offsets to 6000 m, amplitude variation with offset and azimuth (AVOA) may be effective to delineate and characterize fracture zones within Unayzah-A and Unayzah-C reservoirs. The current study was undertaken to determine the improvement of wide azimuth seismic data in fracture detection, especially in clastic reservoirs. For this purpose, the results were validated with available well data including borehole images, well testing and production data in the Unayzah-A. There are no production data or borehole images within the

Unayzah-C, and for validation we had to refer to a comparison of alternative seismic fracture detection methods: mainly curvature and coherence.

Anisotropy was found to be very weak in both reservoirs, with an ellipticity ratio of less than 1, which may be due to noise, clastic lithology and heterogeneity of the reservoirs. Only a few locations have an ellipticity ratio of more than 1, which are located along the western steep flank of the study area. These may correspond to some potential N-S trending faults suggested by circulation loss and borehole image data in few wells. The orientation of the ellipses is NW-SE and is not in agreement with the N-S structural trend. No correlation was found between curvature, coherence and AVOA in Unayzah-A or Unayzah-C reservoirs. Some possible explanation for the low correlation between AVOA ellipticity and natural fractures are noisy dataset, overburden anisotropy, reservoir heterogeneity, granulation seams and deformation.

ABSTRACT (ARABIC)

ملخص الرسالة

الاسم الكامل: علي حسن محمد القواص

عنوان الرسالة: الكشف عن الشقوق بإستخدام تباين سعة الموجة السيزمية مع الإزاحة (AVOA) في مكمن فتاتي، شرق وسط المملكة العربية السعودية

التخصص: الجيوفيزياء

تاريخ الدرجة العلمية: مايو 2015

مكمن العنيزة (C) المتكون في أواخر العصر الكربوني في شرق وسط المملكة العربية السعودية هو مكمن عميق ومنخفض المسامية وربما متشقق. إنه تحد لعالم الجيولوجيا لتعيين أعلى وأسفل مكمن عنيزة (C) بسبب انخفاض نسبة الإشارة إلى الضوضاء (SNR) وعرض النطاق الترددي المحدود في البيانات السيزمية ثلاثية الأبعاد التقليدية. ومن التحديات ذات الصلة، وصف وتحديد مناطق الشقوق داخل مكمن عنيزة (C). للتغلب على تلك التحديات، تم الحصول على البيانات السيزمية ثلاثية الأبعاد ذات النطاق الواسع باستخدام نقطة الإستقبال، التردد المنخفض الاحتلالات وصولا إلى 2 هرتز، و6 كم هندسة التصحيح. وتشير البيانات الجديدة إلى تحسن كبير في إستمرارية البيانات، مما يؤدي إلى تحسين الخرائط للجزء العلوي من مكمن عنيزة (C).

تقنية "تباين سعة الموجه السيزمية" (Azimuthal Amplitude Variation with Offset) قد تكون فعالة لوصف وتحديد مناطق الشقوق داخل مكمن عنيزة (A) ومكمن عنيزة (C). أجريت الدراسة الحالية لتحديد تحسين البيانات السيزمية واسعة السمت في مجال الكشف عن الشقوق، خصوصاً في المكامن الفتاتية. لهذا الغرض، تم التحقق من صحة النتائج مع البيانات المتاحة بما في ذلك صور أسفل الآبار (borehole images)، واختبار الآبار (well testing) وبيانات الإنتاج في مكمن عنيزة (A). لا توجد بيانات عن الإنتاج أو صور أسفل الآبار داخل مكمن عنيزة (C)، وللتحقق من صحة النتائج كان علينا مقارنتها مع نتائج أساليب بديلة للكشف عن الشقوق باستخدام البيانات السيزمية مثل (curvature and coherence).

لقد وجد أن التباين ضعيف جدا في كل من المكمنين بنسبة أقل من 1، الذي قد يكون ناجماً بسبب الضوضاء والخصائص التفتتية الصخرية وعدم تجانس في المكامن. فقط عدد قليل من المواقع لديها نسبة الإهليليجية أكثر من 1،

والتي تقع على طول الجهة الغربية الحادة لمنطقة الدراسة. قد تتوافق هذه مع الصدع في الاتجاه الشمالي - الجنوبي حسب البيانات في عدد قليل من الآبار. اتجاه الحذف هو شمال غربي – جنوب شرقي لا يتفق مع الاتجاه الهيكلي شمالي – جنوبي. ولم يعثر على أي إرتباط بين (curvature and coherence) وتباين سعة الموجه السيزمية (AVOA) في عنيزة (A) أو مكمن عنيزة (C). بعض التفسيرات المحتملة للارتباط المنخفض بين تباين سعة الموجه السيزمية (AVOA) والشقوق الطبيعية هي ارتفاع الضوضاء في البيانات السيزمية، تباين التثاقل على المكمن، عدم تجانس المكمن، طبقات التحبيب وتشوه.

CHAPTER 1

INTRODUCTION

Open fractures in low porosity media have a significant influence on the movement of fluid during production. In addition, they may provide additional limited storage for hydrocarbon. Therefore, the prediction of fracture position, orientation and intensity has become important in the characterization of tight reservoirs to optimize drilling locations and plan future field development.

Fracture detection and modeling can be conducted using well data successfully in mature fields, but in exploration or newly developing fields with few wells, seismic data is the main and perhaps the only means to predict fractures. There are several different approaches to extract fracture information from seismic and each has been widely applied with varying degrees of success. The objective of this thesis is to test the Amplitude Variation with Offset and Azimuth (AVOA) technique in a deep-seated clastic reservoir in a gas field in Eastern Central Saudi Arabia.

One of the challenging tasks in Unayzah-C fracture evaluation is to map the top of these low permeability and low porosity sandstones due to low signal-to-noise ratio (SNR) for very deep reflections in the seismic section. A related challenge is to delineate and characterize open fracture zones within the Unayzah-C reservoir to optimize drilling locations. Conventional narrow azimuth 3D seismic data used in the past have failed to resolve these issues due to limited bandwidth and low SNR from contamination by

interbed and surface-generated multiples, particularly for the deep-targeted Unayzah-C reservoir in the study area. In addition, the lack of full-azimuth information in the conventional seismic data has limited the analysis of fracture detection techniques such as AVOA. Now a new 3D full-azimuth broadband seismic dataset is available and our study is based on this new data.

CHAPTER 2

SEISMIC FRACTURE PREDICTION

There are several techniques for indirectly extracting fracture information from seismic such as measuring shear-wave (S-wave) splitting, AVOA, azimuthal variations in primary-wave (P-wave) velocity, and post-stack techniques such as coherence and curvature analysis. Historically, seismic fracture prediction has concentrated on S-wave data. The first to describe S-wave splitting caused by fractures from earthquake data was Crampin et al. (1980). Alford (1986) studied S-wave splitting and concluded that when processing S-wave data, azimuthal anisotropy should be taken into consideration to enhance data quality. He demonstrated that when an S-wave propagates through a fracture, it splits into a fast S-wave parallel to the fracture and a slow S-wave perpendicular to the fracture, referred to as S-wave splitting. Many studies of S-wave splitting have been done on S-wave data for fracture analysis (e.g., Lynn and Thomsen, 1990; Lefeuvre et al., 1992; Thomsen et al., 1995).

Unfortunately, recording and processing S-wave data is significantly more complicated and expensive than the acquisition of P-wave data. Besides, the S-wave does not transmit through fluid media therefore; they are not usable in offshore field studies unless an ocean bottom cable (OBC) survey is used. For these reasons, the use of P-wave seismic data has recently drawn greater attention for use in fracture detection and analysis. Many studies have been published on fracture analysis using P-wave data (e.g., Thomsen, 1986;

Rüger and Tsvankin, 1997; Al-Shuhail, 1998; Al-Hawas et al., 2003; Al-Shuhail, 2004; Al-Shuhail, 2007; Al-Dajani, 2008; Balhareth, 2009; Alqahtani and Al-Shuhail, 2013).

A combination of different techniques is the best approach for achieving confidence in predicting fractures (Figure 2.1) since there is no particular technique that works best all the time (Treadgold et al., 2008). Al-Marzoug et al. (2006) showed a large variation in AVOA and a small azimuthal variation in P-wave velocity on two case studies in Saudi Arabia. They concluded that AVOA is more reliable than azimuthal variations in P-wave velocity for predicting anisotropy related to fracture presence.

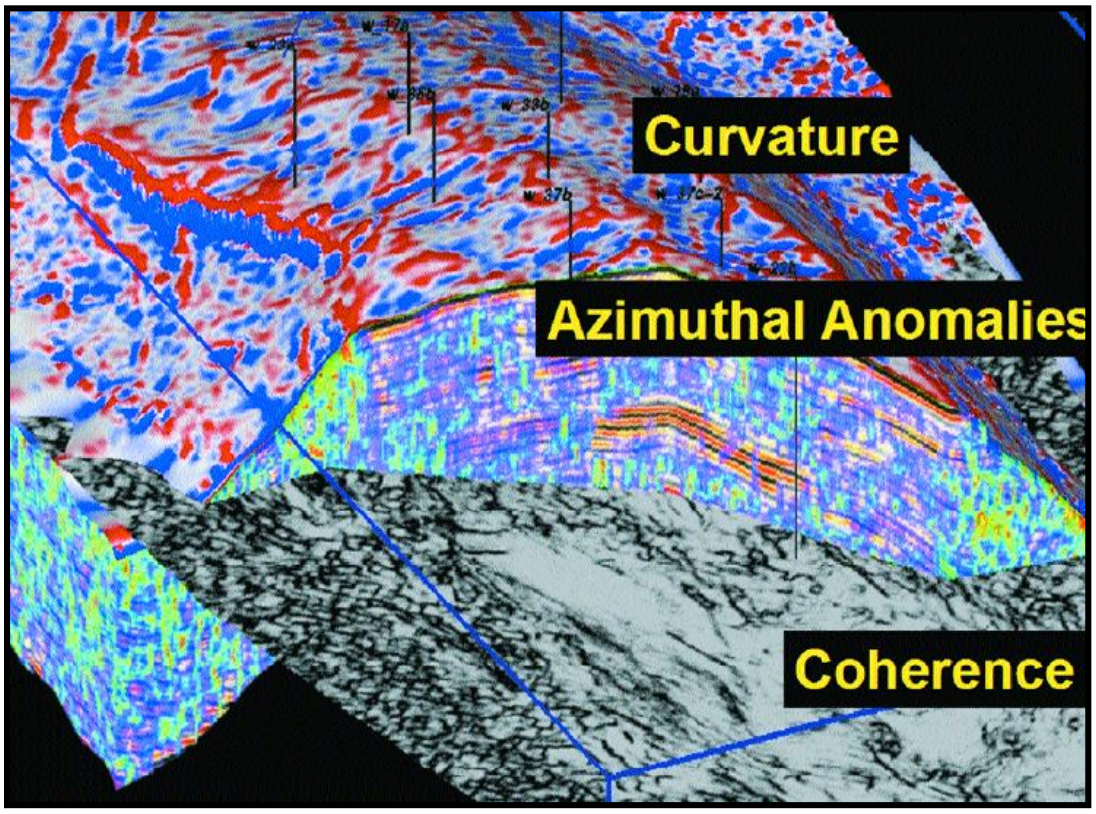

Figure 2-1 - Combination of different techniques to predict fractures (Treadgold et al, 2008).

2.1 Amplitude Variation with Offset (AVO) Technique

When an incident P-wave encounters an interface between two layers, a portion of its energy is reflected and the rest of the energy is transmitted to the lower medium. The incident P-wave generates four different waves at the interface. These are reflected and transmitted P-waves and reflected and transmitted S-waves (Figure 2.2). Snell's Law explains the angles of different wave-generated modes as a function of their velocities. Zoeppritz (1919) derived equations to explain the amplitudes of different wave-generated modes as functions of their P-wave velocity, S-wave velocity, density, angle of incidence, angle of reflection, and angle of transmission. The reflection coefficients are the ratio of the reflected wave amplitudes to the incident wave amplitude and the transmission coefficients are the ratio of the transmitted wave amplitudes to the incident wave amplitude. I will be discussing only the reflected P-wave case in this study.

For a normal incidence P-wave, Zoeppritz equation for the P-wave reflection coefficient (R) between two layers of densities ρ_1 and ρ_2 and velocities V_{P1} and V_{P2} of the first and second layer respectively is simplified to:

$$R = \frac{\rho_2 V_{P2} - \rho_1 V_{P1}}{\rho_2 V_{P2} + \rho_1 V_{P1}} \tag{1.1}$$

In the case of non-normal incidence, the Zoeppritz equations become very complicated. The complexity of the Zoeppritz equations has resulted in a number of approximations such as those developed by Aki and Richards (1980), Ostrander (1984) and Shuey (1985) to simplify the relationship between the reflection coefficient and angle of incidence.

Aki and Richards (1980) simplified the Zoeppritz equation by assuming a small change in elastic properties across the interface between two layers and assuming that the incidence angle was less than the critical angle. The Aki and Richards (1980) approximation becomes:

$$R(\theta) = \left[\frac{1}{2}\left(1 - 4\frac{V_S^2}{V_P^2}\sin^2\theta\right)\right]\frac{\Delta\rho}{\rho} + \left[\frac{1}{2\cos^2\theta}\right]\frac{\Delta V_P}{V_P} - \left[4\frac{V_S^2}{V_P^2}\sin^2\theta\right]\frac{\Delta V_S}{V_S} \quad (1.2)$$

where

$$\Delta V_P = (V_{P2} - V_{P1})$$

$$\Delta V_S = (V_{S2} - V_{S1})$$

$$\Delta\rho = (\rho_2 - \rho_1)$$

$$V_P = \frac{(V_{P2} + V_{P1})}{2}$$

$$V_S = \frac{(V_{S2} + V_{S1})}{2}$$

$$\rho = \frac{(\rho_2 + \rho_1)}{2}$$

and

$$\theta = \frac{(\theta_2 + \theta_1)}{2}.$$

Shuey (1985) modified Aki and Richards (1980) equation by expressing the properties in terms of Poisson's ratio σ and $\Delta\sigma$. This led to a 3-term Shuey's approximation of Zoeppritz equations:

$$R(\theta) = R_0 + G\sin^2\theta + F(\tan^2\theta - \sin^2\theta) \quad (1.3)$$

where

$$R_0 = \frac{1}{2}\left[\frac{\Delta V_P}{V_P} + \frac{\Delta\rho}{\rho}\right] \quad (1.4)$$

describes the variation of reflection amplitudes at normal incidence ($\theta = 0°$),

$$G = A_0 R_0 + \frac{\Delta\sigma}{(1-\sigma)^2} \quad (1.5)$$

describes the variation of reflection amplitudes at intermediate offset ($\theta \leq 30°$),

where

$$A_0 = B - 2(1+B)\frac{1-2\sigma}{1-\sigma} \quad (1.6)$$

$$B = \frac{(\Delta V_P/V_P)}{(\Delta V_P/V_P)+(\Delta\rho/\rho)} \quad (1.7)$$

and

$$F = \frac{1}{2}\frac{\Delta V_P}{V_P} \quad (1.8)$$

describes the variation of reflection amplitudes at offsets approaching the critical angle. Shuey further simplified this approximation by assuming that the offset is small when the angle of incidence is less than 30° so the third term (F) will go to zero leading to:

$$R(\theta) = R_0 + G\sin^2\theta \quad (1.9)$$

This equation is called the AVO equation. R_0 is called the AVO intercept and G is called the AVO gradient. The AVO equation explains the amplitude variation with offset for an isotropic medium.

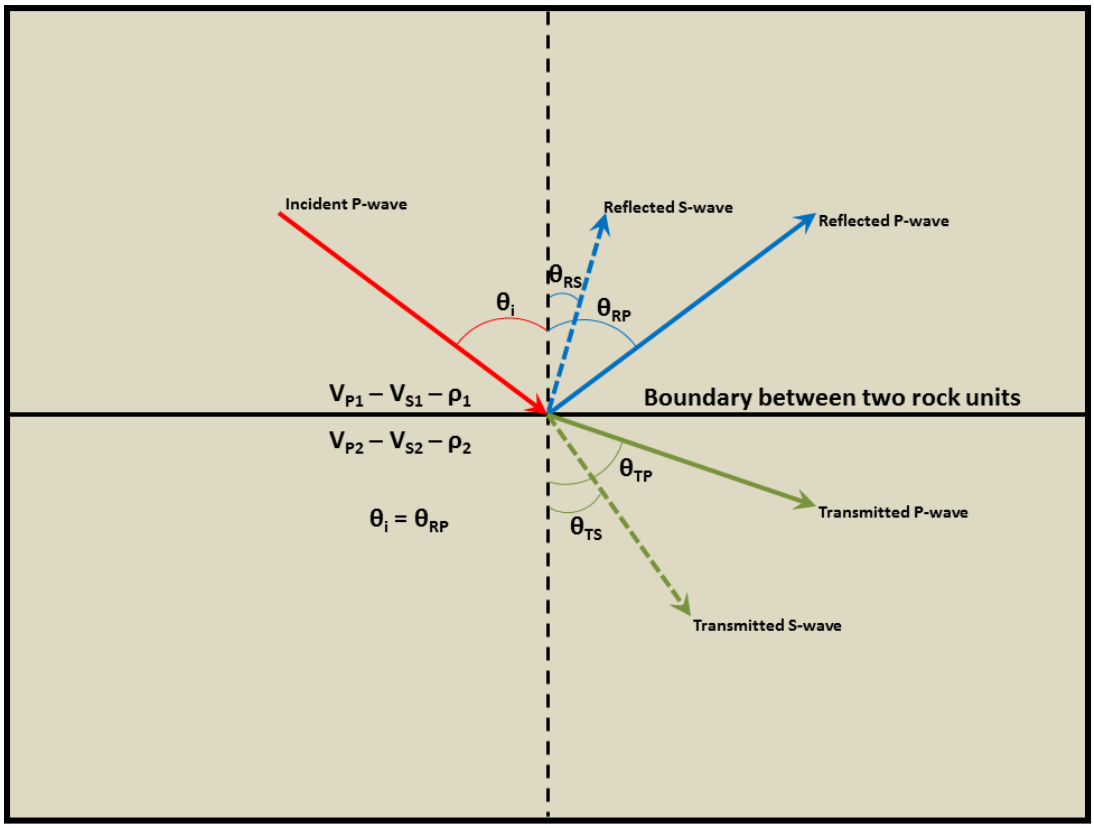

Figure 2-2 - Reflected and transmitted waves generated by an incident P-wave.

2.2 Amplitude Variation with Offset and Azimuth (AVOA) Technique

For an anisotropic medium, the AVO equation (1.9) has to be reformed to account for the effect of anisotropy. Rüger and Tsvankin (1997) indicated that the effect of fractures will be seen in the AVO gradient, but will not impact the AVO intercept. They reformed the AVO equation (1.9) to compute AVOA as:

$$R(\theta, \phi) = R_0 + [G_{iso} + G_{anis} \cos^2(\phi - \beta)] \sin^2 \theta \qquad (1.10)$$

for angles of incidence less than or equal to 30°, where $R(\theta, \phi)$ is the reflection coefficient as function of incidence angle (θ) and the source-receiver azimuth (ϕ), R_0 is the AVO intercept. $G_{iso}$is the isotropic AVO gradient and G_{anis} is anisotropic AVO gradient. β is the azimuth perpendicular to the fracture direction.

If there is no azimuthal anisotropy then the AVO response will be the same for all azimuths. However, if there is azimuthal anisotropy then the AVO response will be different from one azimuth to another. Figure 2.3 illustrates the impact of a fractured reservoir over AVO and AVOA on the stack response (Williams and Jenner, 2002). Figure 2.4 illustrates the effect of aligned fractures on the elasticity and reflectivity of a medium and clarifies the 2D AVO and AVOA concepts (Hall et al., 2002). To clarify the concept of AVOA further, Figure 2.5 shows AVOA curves for a target horizon for a CDP gather for a range of azimuths. Notice the large variation in the AVO gradient with azimuth (Neves el al., 2003).

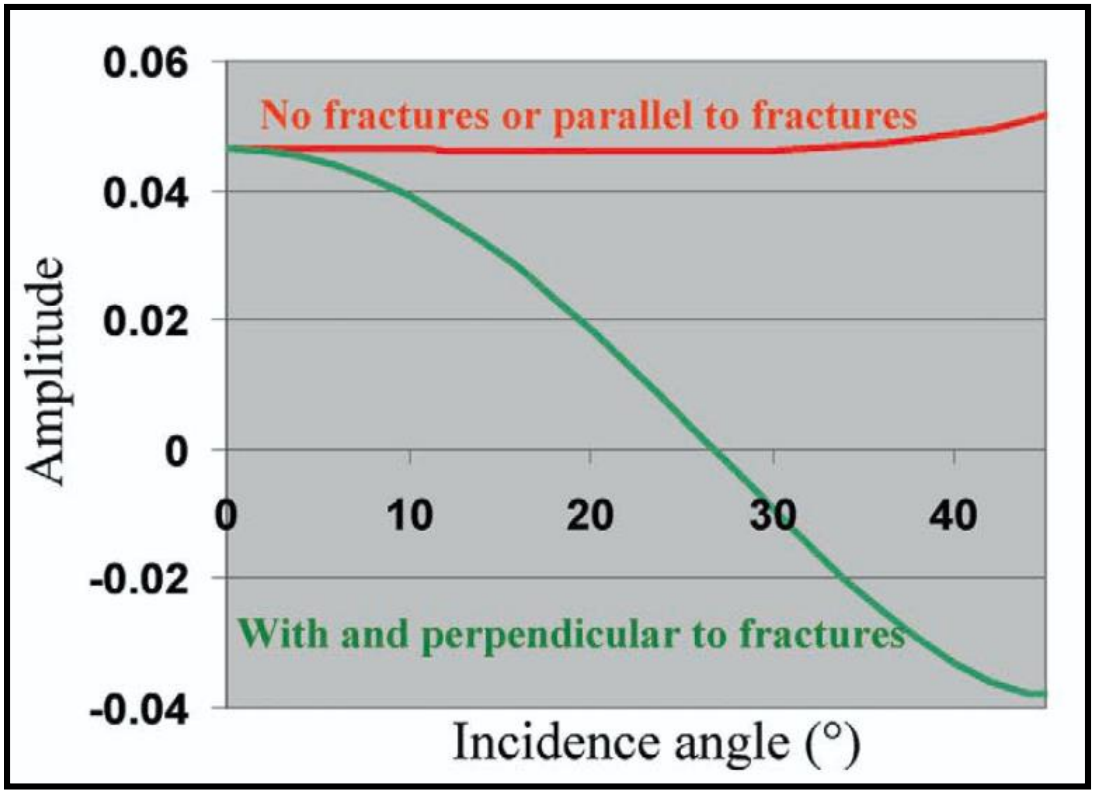

Figure 2-3 - The amplitude response versus incidence angle for a particular carbonate-carbonate interface. When wave propagation direction is parallel to the fractures or if both layers are non-fractured then there is a little AVO response (red curve). When wave propagation is perpendicular to the fractures then a strong AVO response (green curve) is observed (Williams and Jenner, 2002).

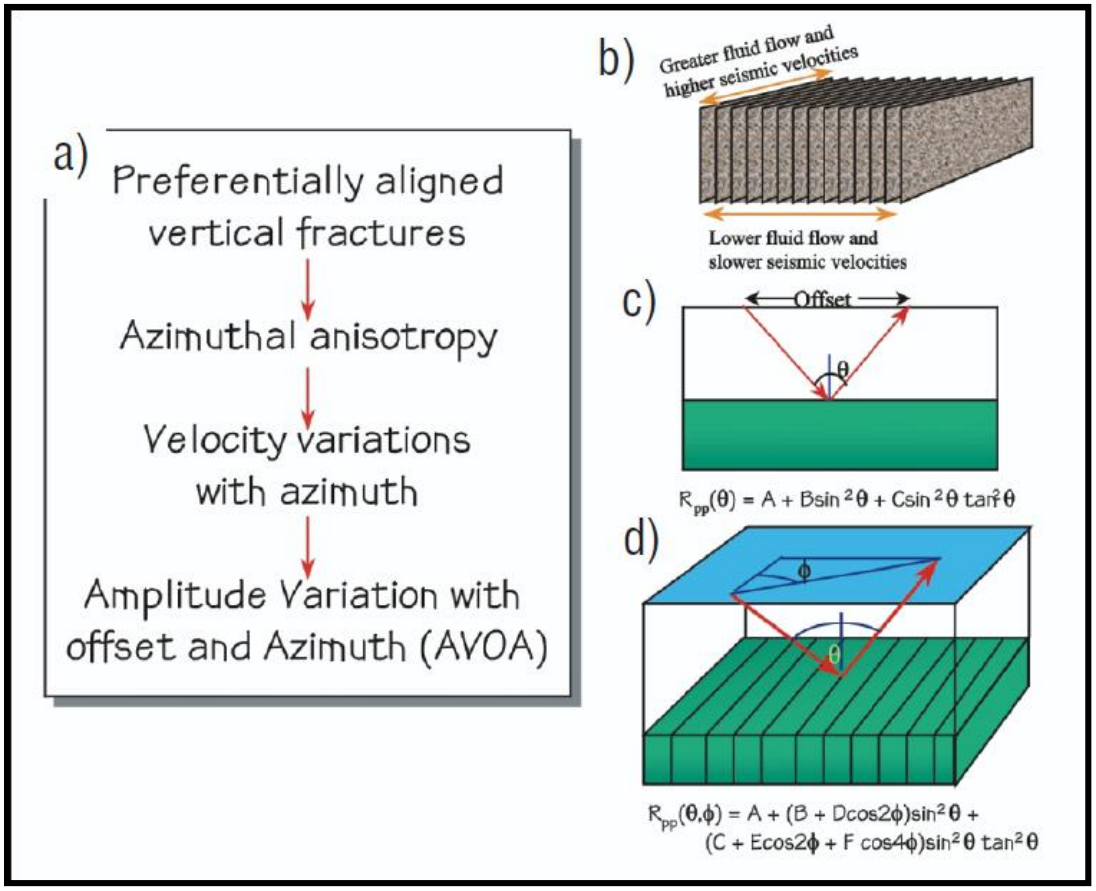

Figure 2-4 - a-b) The effect of aligned fractures on the elasticity and reflectivity of a medium. c) 2D AVO principle. d) AVOA principle (Hall el al., 2002)

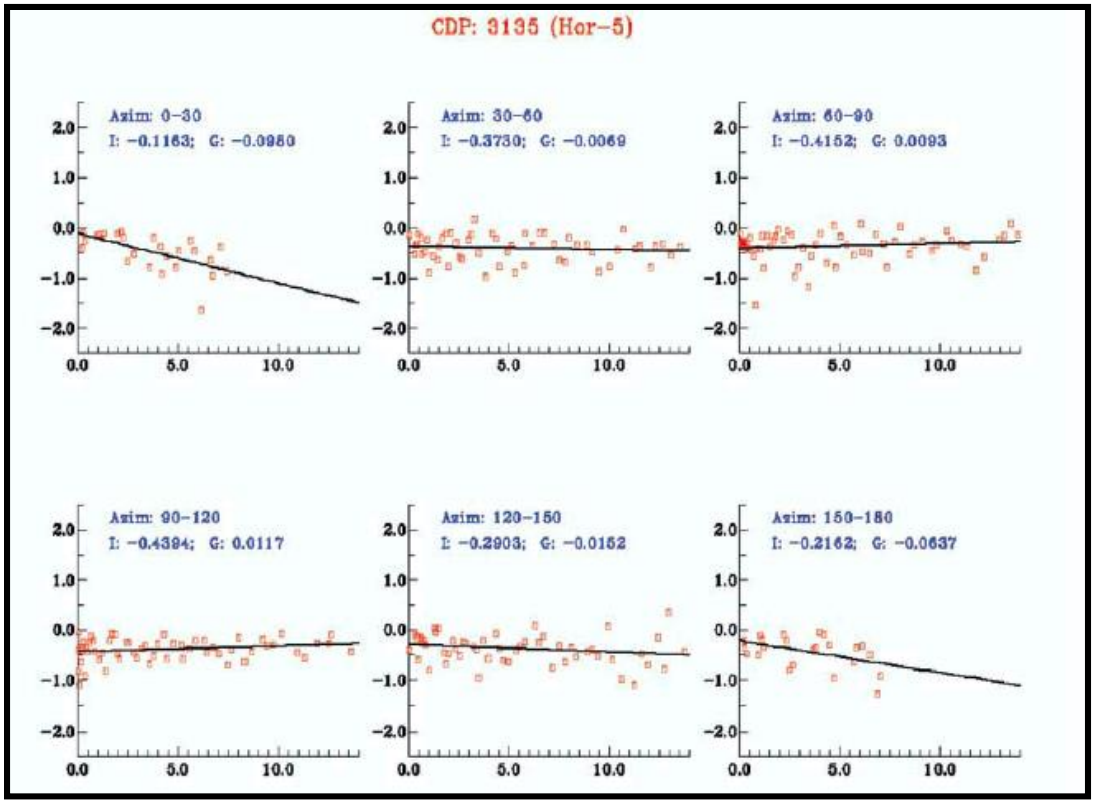

Figure 2-5 - Variation of AVOA computed from seismic data at top reservoir for a CDP gather (Neves et al., 2003)

2.3 Ellipse Fitting Technique

Grechka and Tsvankin (1998) were the first to apply an ellipse fitting technique in the field of azimuthal seismic anisotropy. To perform the ellipse fitting technique, equation (1.10) has to be modified using the polar coordinate system. Jenner (2002) obtained the following from equation (1.10):

$$R(\theta, \phi) = R_0 + [W_{11} \cos^2 \phi + 2W_{12} \cos \phi \sin \phi + W_{22} \sin^2 \phi] \sin^2 \theta \qquad (1.11)$$

where the three coefficients W_{11}, W_{12} and W_{22} represent an azimuthally varying AVO gradient ellipse and ϕ is the source-receiver azimuth. Then equation (1.10) and (1.11) are related as follow (Al-Marzoug et al., 2006):

$$\beta = \tan^{-1}\left[\frac{W_{11}-W_{22}+\sqrt{(W_{11}-W_{22})^2+4W_{12}^2}}{2W_{12}}\right] \quad (1.12)$$

$$G_{max} = \frac{1}{2}\left(W_{11} + W_{22} + \sqrt{(W_{11}-W_{22})^2 + 4W_{12}^2}\right) \quad (1.13)$$

$$G_{min} = \frac{1}{2}\left(W_{11} + W_{22} - \sqrt{(W_{11}-W_{22})^2 + 4W_{12}^2}\right) \quad (1.14)$$

where β is the minimum gradient (G_{min}) azimuth from zero azimuth (north direction), G_{max} represents the major ellipse axis and G_{min} represents the minor ellipse axis (Figure 2.6).

Now we can measure the ellipticity (E), which is the measure of anisotropy that could be related to the presence of fractures by the ratio:

$$E = \frac{G_{max}-G_{min}}{G_{min}} \quad (1.15)$$

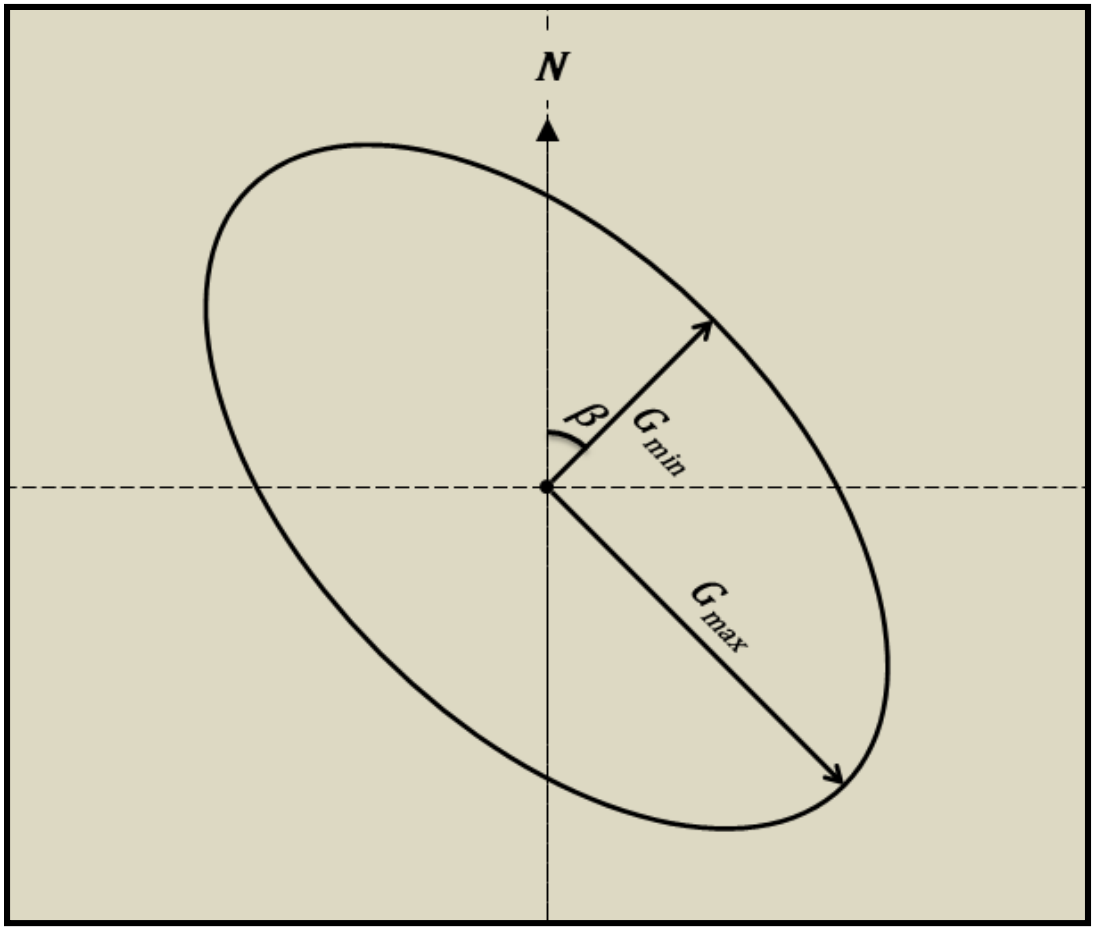

Figure 2-6 - The AVOA curve-fitting technique.

2.4 Other Seismic Techniques

Coherence and curvature attributes are produced from post-stack seismic data that can assist the analysis of fracture detection. Coherence is a measure of the similarity of a trace to its surrounding traces (Sheriff, 2002). Therefore, the coherence along discontinuities decreases significantly highlighting structural fractures and faults and stratigraphic channels and reefs on the seismic data. Curvature is computed to emphasize the changes in shape of the surface corresponding to faults, fractures, folds and depositional features.

CHAPTER 3

METHODOLOGY

3.1 Workflow

The top of the Unayzah-C reservoir is mapped using the newly acquired 3D full-azimuth broadband seismic data. The mapped surface is used in the AVOA analysis to determine areas of high fracture potential area. The results achieved through the AVOA methodology should constrain the existence of fractures away from well control.

The Unayzah-C reservoir was never mapped directly using the original conventional 3D seismic data due to contamination from interbed multiples, limited bandwidth, and the resultant low SNR. There was no seismic signature to define the top and base of the reservoir, because the seismic data were obscured by interbed multiples and random noise. As an alternative, the base of the Khuff carbonate reflection was used as a proxy for the top of the reservoir (Wallick and Giroldi, 2013). In addition, delineation and characterization of fractures have not been directly measured from stacked seismic amplitude volumes to date.

In 2010, a new 3D full-azimuth broadband seismic dataset was acquired over the study area. The uplift in bandwidth and improved SNR are a result of improved acquisition parameters and include the use of point receivers allowing high-density wavefield sampling to 12.5 m, low frequency sweeps down to 2 Hz, and full-azimuth offsets to 6000 m in a full-azimuth patch (Pecholcs et al, 2012; Wallick and Giroldi, 2013). The

acquisition parameters were designed to enhance imaging of the subsurface data and to reveal reservoir properties information. The symmetric sampling of the data is appropriate for offset vector tile (OVT) sorting (Cary, 1999; Vermeer, 2002), which was used in the processing workflow to preserve azimuthal information in the PreStack Time Migration (PSTM) gathers for AVOA analysis.

3.2 Presentation of Results

The AVOA technique was applied to Unayzah-C and Unayzah-A reservoirs and the results are presented as three fundamental maps:

1. Ellipse long axis as sticks
2. Anisotropy ratio as color code
3. Anisotropy orientation as color code

The results are also displayed on seismic profiles to show vertical anisotropy and orientation variation.

3.3 Validation

Seismic techniques do not provide direct fracture information but only indicators, which must be validated and calibrated with actual data. The two main parameters provided by anisotropy analysis are anisotropy ratio and orientation of the anisotropy ellipse at each grid location. Borehole image logs provide actual fracture orientation and density and hence are the best means to validate anisotropy ellipses as fracture density and strike

indicators. Well testing is another important source of fracture information. Well tests identify not only faults but also diffuse fractures and their permeability, porosity and matrix block size, which can be correlated with seismic anisotropy (Ozkaya, personal communication). Wells with homogeneous matrix interpretation cannot have fractures within the radius of investigation. Initial productivity index is among several other fracture indicators and can be correlated with seismic anisotropy.

Unfortunately, image logs and dynamic data are available only from the Unayzah-A reservoir, which is the main producing reservoir, and little or no well data are available from the Unayzah-C reservoir. Therefore, it was decided to correlate fracture anisotropy results with other seismic fracture indicators such as curvature and coherence over the reservoir zone. The primary objective of coherence and curvature is detection of faults, but because faults are often associated with fractures, these methods could provide information of fault related fracture orientation and density variation.

Several overlay maps were also generated, displaying anisotropy sticks along with rose diagrams from borehole image logs, anisotropy ratio, an overlay of homogeneous matrix wells from well tests for the Unayzah-A reservoir. Comparative maps were prepared showing curvature and coherence maps along with anisotropy maps for Unayzah-C reservoir. In addition to maps, the long axis of anisotropy ellipses were extracted and rose diagrams were prepared to compare with the actual fracture rose diagrams from borehole image logs.

CHAPTER 4

GEOLOGICAL SETTING

4.1 Reservoir Description

In Eastern Central Saudi Arabia, the late Carboniferous-early Permian Unayzah Formation is underlain by rocks of the Devonian-Carboniferous Jubah Formation and overlain by the Permo-Triassic Khuff Formation (Melvin and Sprague, 2006). The Unayzah Formation is bounded by two major unconformities that separate it from the underlying and overlying formations. The lower bounding contact is the Hercynian unconformity and the upper bounding contact is the pre-Khuff unconformity (Melvin and Sprague, 2006; Melvin and Norton, 2013). The Unayzah Formation is widespread in the Greater Arabian basin and is subdivided into four members from oldest to youngest: Unayzah-C member, Unayzah-B member, Unnamed Unayzah member and Unayzah-A member (Melvin and Sprague, 2006, Melvin et al., 2010). All four members of the Unayzah Formation in the subsurface are bounded by depositional hiatuses (Melvin and Norton, 2013). In this thesis, I only focus on the Unayzah Formation over a study area in Eastern Central Saudi Arabia.

In the study area (Figure 4.1), the Unayzah-C member is comprised of quartz-cemented sandstones that were deposited during a retreat phase of the earliest stages of late Paleozoic Gondwanan glaciation (Melvin and Sprague, 2006 and Melvin and Norton, 2013). Figure 4.2 shows that the Unayzah-C member is underlain unconformably by the

Silurian Qusaiba member of the Qalibah Formation and overlain unconformably by the Permian Unayzah-A member (Melvin and Sprague, 2006). Following the glacial retreat phase, several phases of glacial advances, retreats, and re-advances of the ice sheets occurred (Melvin and Sprague, 2006 and Melvin et al., 2010). During these phases, sediments were deposited and thrust over each other forming a number of stacked, low-angle thrusted, push moraine features separated by distinct shear zones (Melvin et al., 2010; Melvin and Norton, 2013). According to Melvin and Sprague (2006) and Melvin et al. (2010), the distinctive sub-horizontal shear zones in the Unayzah-C member have been observed in cores in several wells in Central Saudi Arabia and range in thickness from 2 ft to over 20 ft. These shear zone features have not been observed in the adjacent rock units (Melvin and Norton, 2013). The distinct shear zone features of the Unayzah-C member may act to compartmentalize hydrocarbon within the reservoir (Melvin and Norton, 2013). Unayzah-C member appears as a poorly bedded and very heterogeneous unit on borehole image logs (Figure 4.3)

The Unayzah-A member is very different from the glacial deposits of Unayzah-C member and consists mainly of cross bedded eolian dune sandstones, which grade to fine grained ephemeral lake sediments toward the south (Melvin et al. 2010; Wallick and Giroldi, 2013). Unayzah-A member is divided into two sub-units. The lower unit is mainly sandstone deposits in fluvial, coastal plain grading to estuarine or shallow marine depositional environment. The Upper unit is mainly eolian sandstone. Figure 4.2 shows that the Unayzah-A member is underlain unconformably by the Carboniferous Unayzah-C member and overlain unconformably by the marginal marine basal Khuff clastics. Unayzah-A member cross bedding is very clear on borehole image logs (Figure 4.4). In

contrast to Unayzah-C member, Unayzah-A member is very well bedded. Unayzah-A member is the main reservoir in this field. Currently all the gas production is from Unayzah-A member and hence all image logs, well tests and other dynamic data are confined to Unayzah-A member.

4.2 Structural Setting

The study area is a small field at the SE corner of the giant Ghawar field. The field produces from clastic reservoirs Unayzah-A and Unayzah-C, but mainly in the Unayzah-A reservoir. The field structure is an asymmetric anticline, with a steeper western flank. Tectonic evolution based on flattened seismic profiles demonstrates that there were at least three phases of deformation: one in Pre-Khuff times, one in Late Cretaceous, and one in Late Tertiary (Figure 4.5). The field consists of two dome-shaped lobes. The main structural high is in the south, which is the focus of this thesis (Figure 4.6).

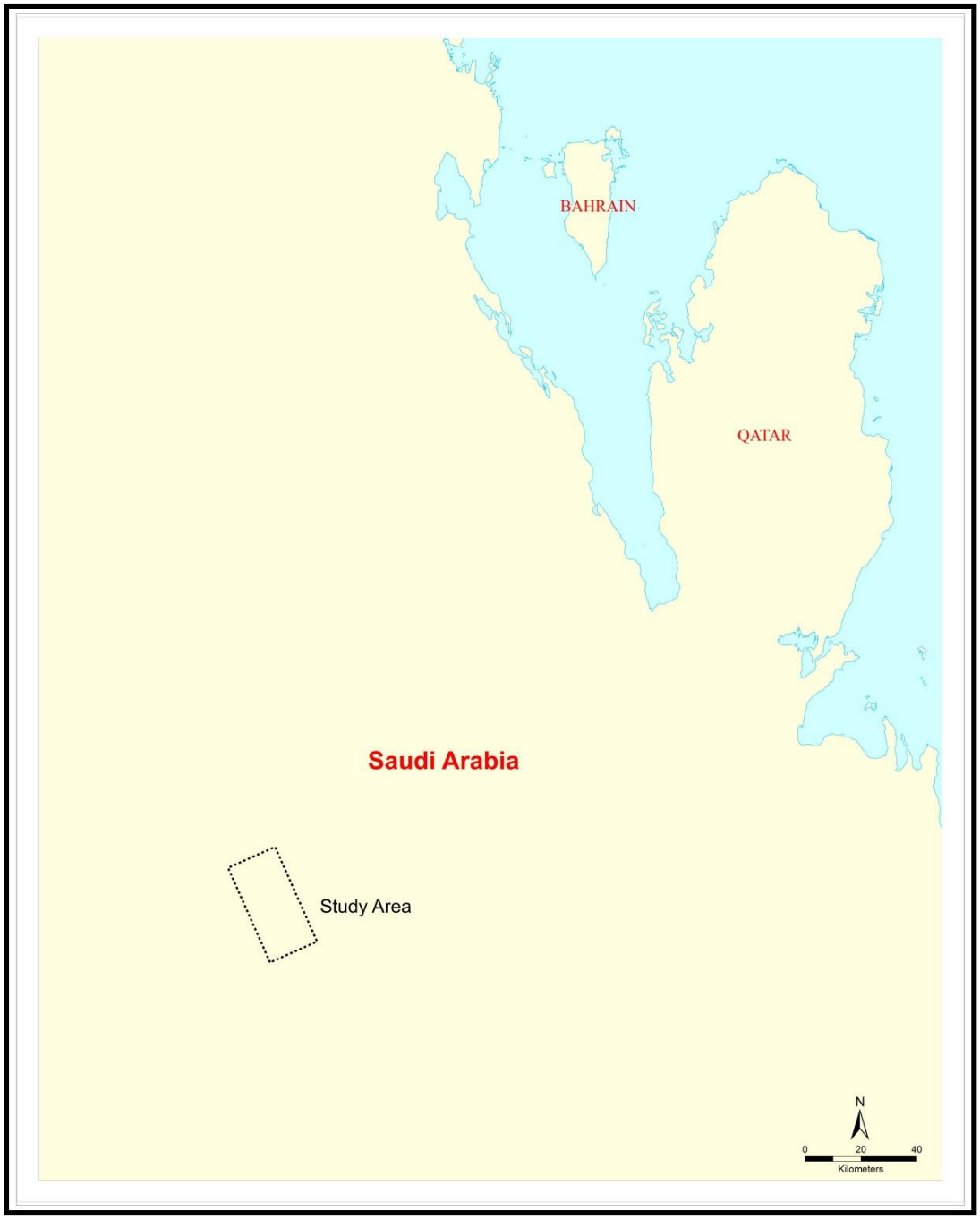

Figure 4-1 - Map of the study area in Eastern Central Saudi Arabia.

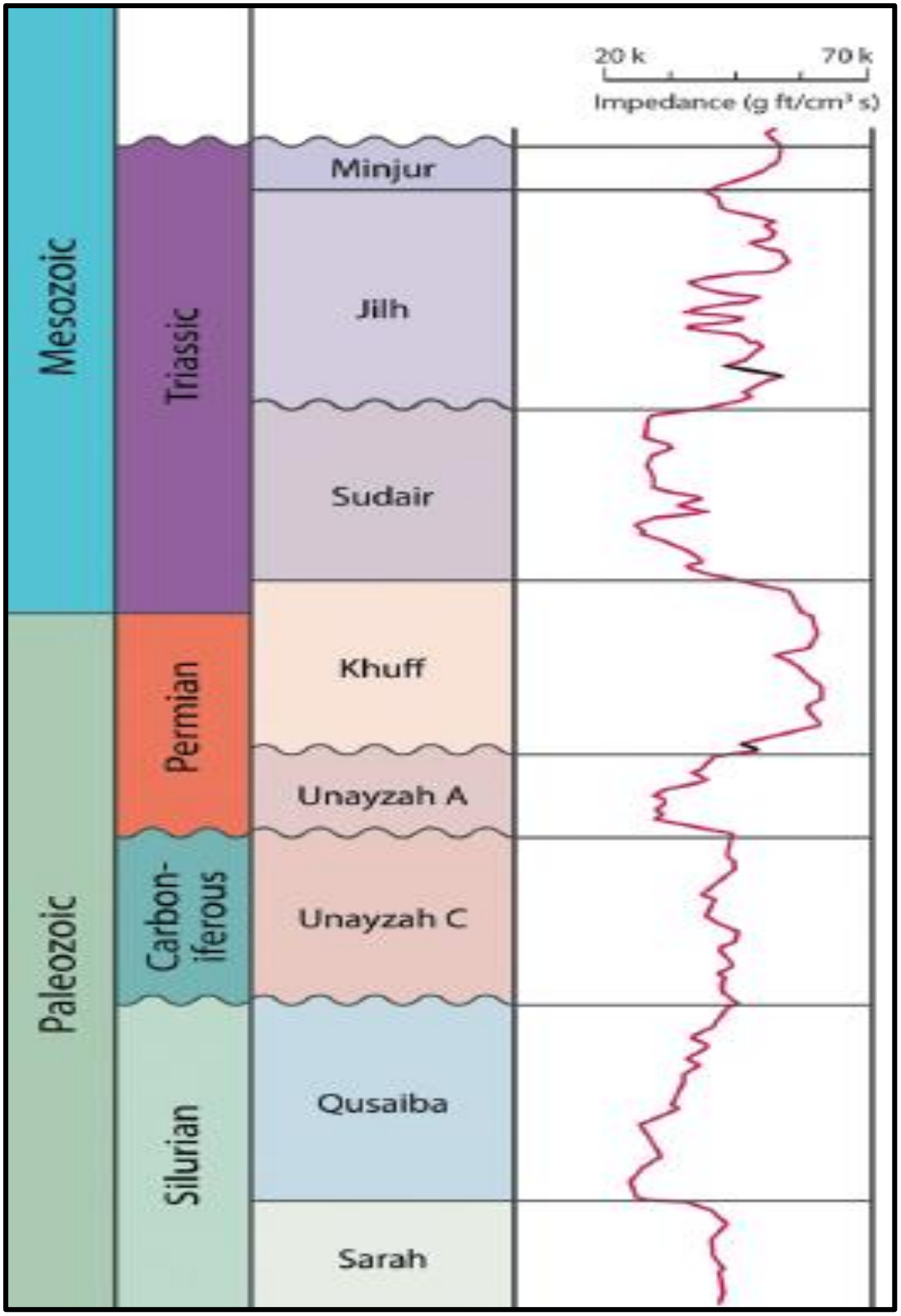

Figure 4-2 - Stratigraphic column of rock units in the study area (Wallick and Giroldi, 2013).

Figure 4-3 - Unayzah-C appears as chaotic and irregular with no or very weak bedding on borehole image logs. The glacial shear zones mentioned in literature cannot be differentiated because of the high degree of heterogeneity but are marked by high Thorium in spectral GR logs.

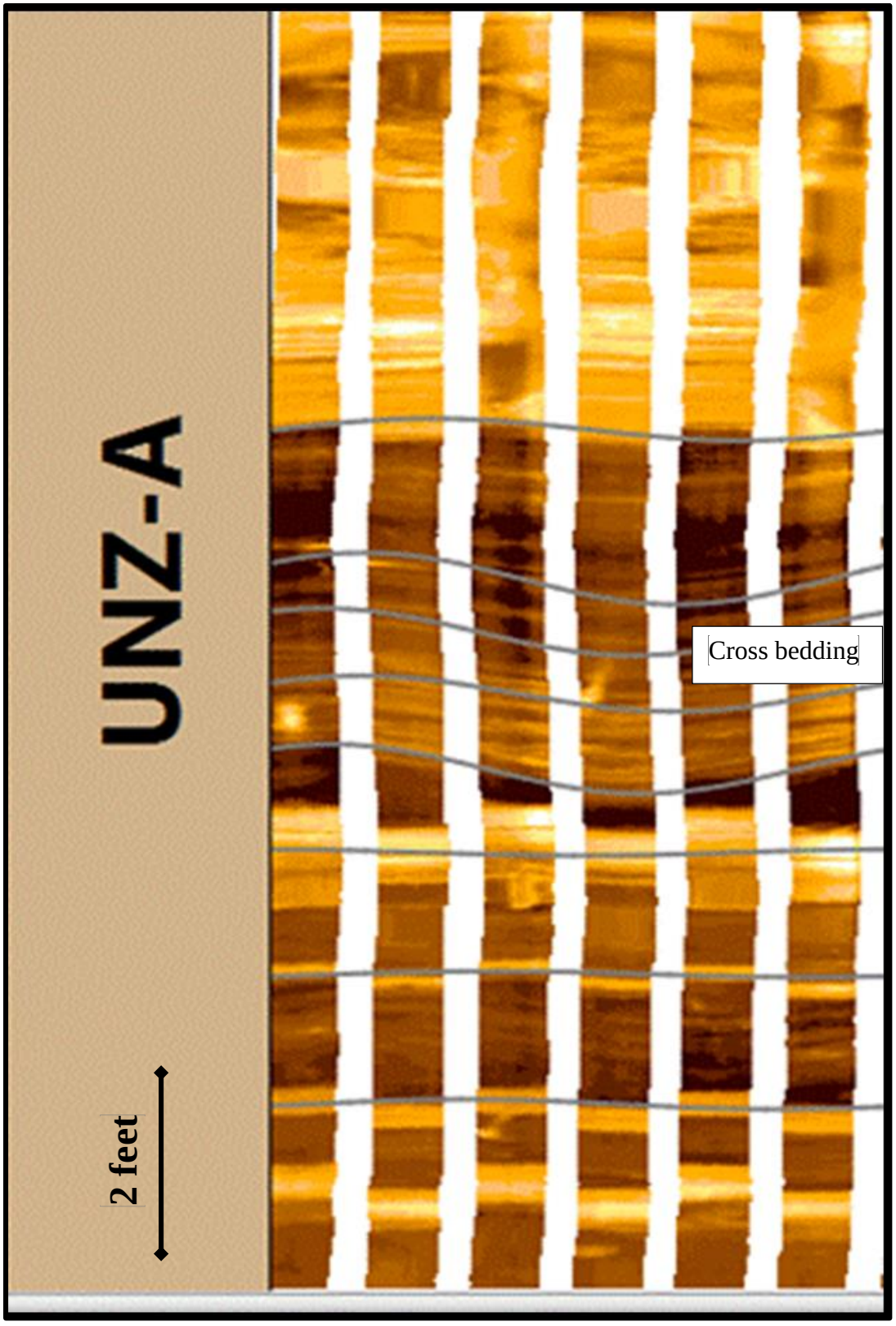

Figure 4-4 - Cross bedding in Unayzah-A from borehole image log of WELL-I. Dominant cross bedding azimuth is N100E.

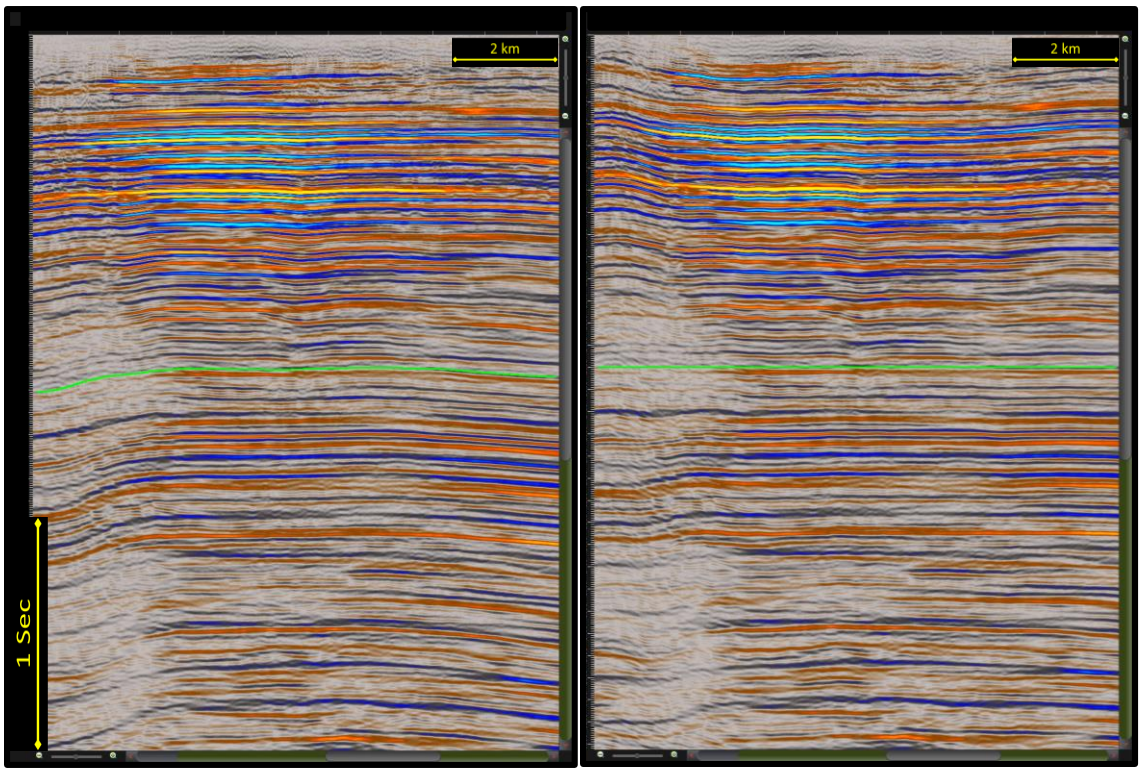

Figure 4-5 - A-EW seismic profile through the field. B- Cross section flattened at Arab-D level.

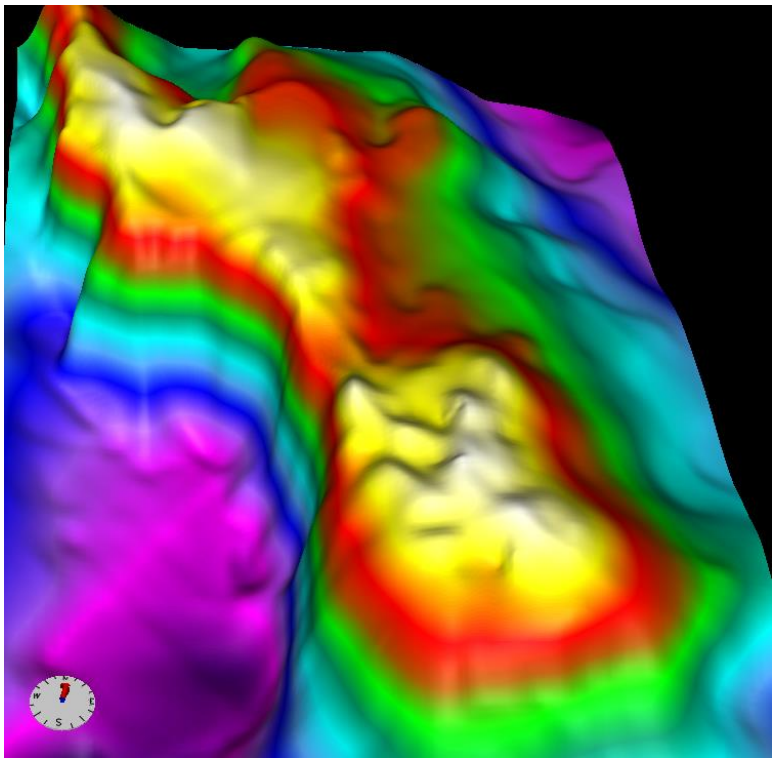

Figure 4-6 - Structure map of top of Unayzah-C member.

CHAPTER 5

SEISMIC DATA ACQUISITION

In 2010, full-azimuth broadband 3D seismic data were acquired over a gas field in Eastern Central Saudi Arabia. The acquisition survey design geometry was orthogonal with high-density wavefield sampling, point receivers, full azimuth, and a vibroseis sweep from 2 Hz to 94 Hz. The spacing of source and receiver lines was 125 m. The spacing of source and receiver group interval was 12.5 m. The patch consisted of 48 receiver lines with maximum inline and maximum crossline offset of 6,000 m. The survey resulted in 46,080 channels at 960 channels per receiver line at a sample rate of 4 ms with a record length time of 6 sec and a nominal fold of 9,216. Table 5.1 lists the detailed acquisition parameters for the survey and Figure 5.1 shows the survey layout. More information about the acquisition can be found in Pecholcs et al. (2012), Wallick et al. (2012) and Wallick and Giroldi (2013).

For the AVOA analysis, the maximum offset was reduced from 8,500 m to around 6,000 m in each bin to achieve the same maximum offset in all azimuths (Figure 5.3 and 5.4). This is an essential step to avoid errors in computing the fracture orientation and intensity due to uneven offset vs azimuth distribution.

Table 5.1 - Survey Acquisition Parameters.

Spread type	WAS-1 Single Sensor 3D - Symmetric Split-Spread
Number of active receiver lines	48
Number of active stations per receiver line	960
Number of traces	46,060
Distance between source lines	125 m
Distance between receiver lines	125 m
Source station interval	12.5 m
Receiver station interval	12.5 m
Inline offset	
Maximum offset	± 6,000 m
Minimum offset	± 6.25
Crossline roll	1 receiver line after each swath
Nominal fold	9,216
Sweep length	12 sec
Frequency range	2-94 Hz
Recording sample rate	4 ms
Record length, uncorrelated	18 sec (12 sec sweep + 6 sec listen)
Record length, correlated	6 sec

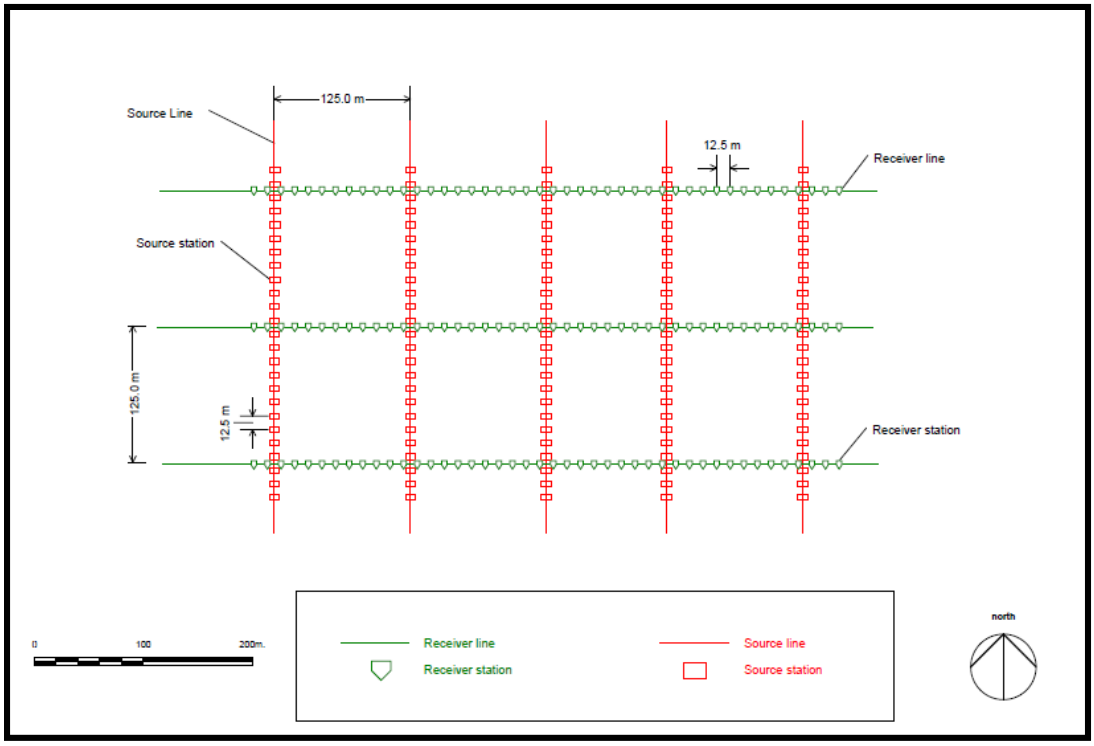

Figure 5-1 - Source and receiver line and station configuration

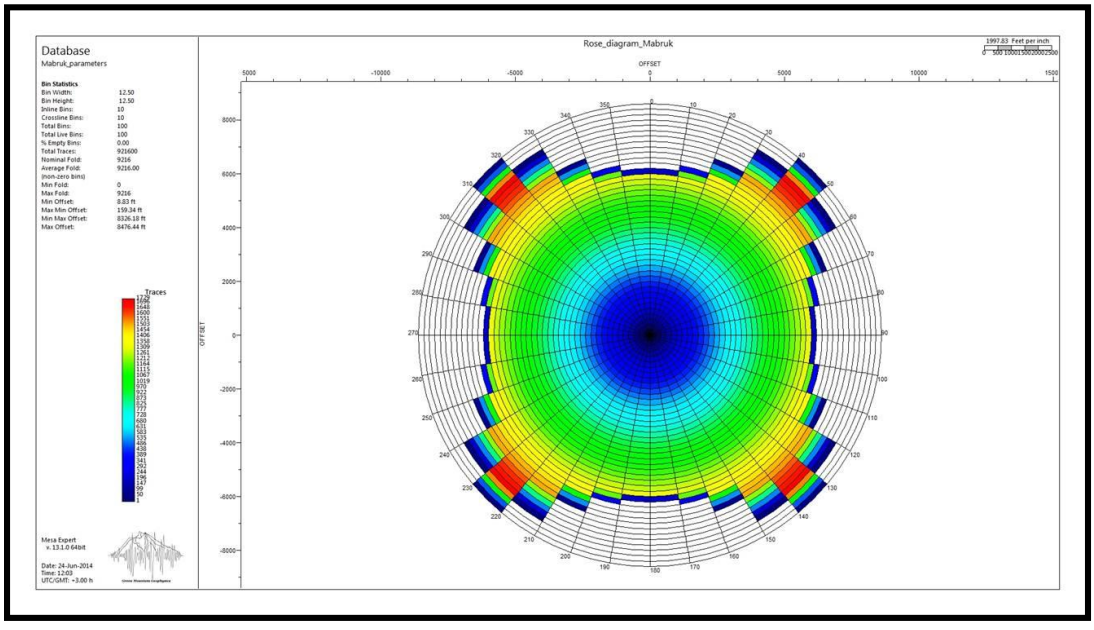

Figure 5-2 - Offset vs. azimuth rose diagram for a CMP bin in the study area. Note that an even distribution is reached if we used no more than 6,000 m offset.

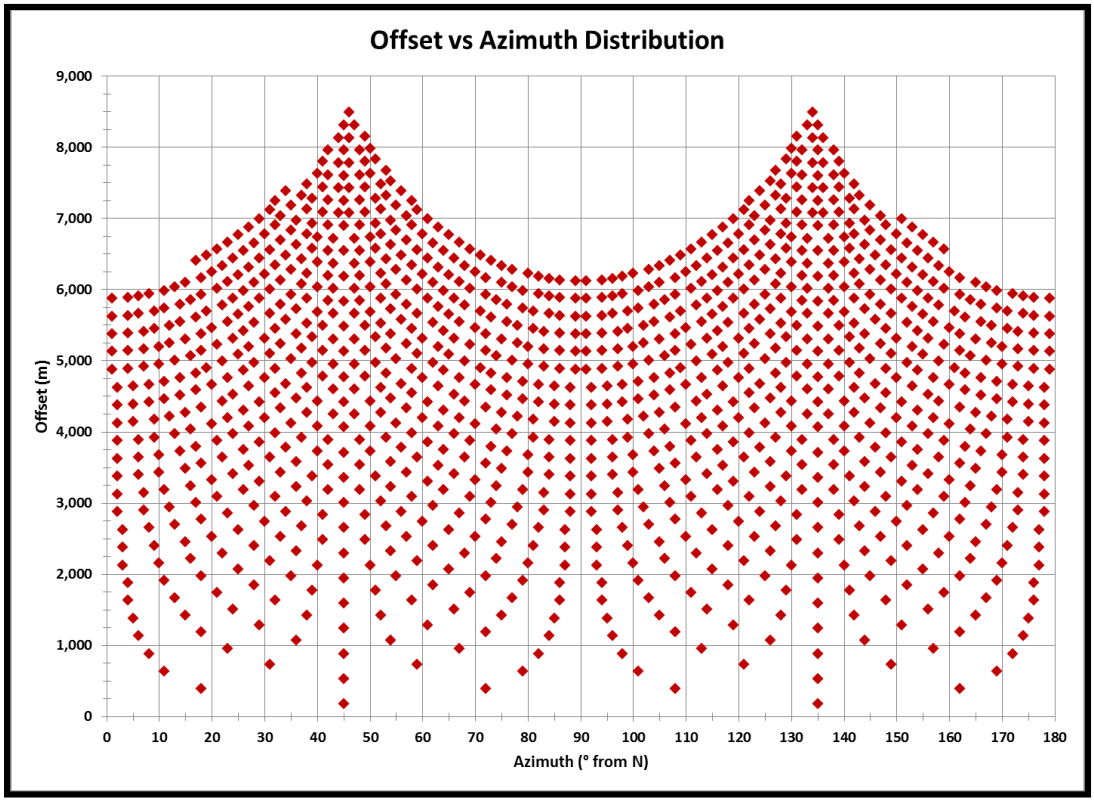

Figure 5-3 - Offset vs. azimuth distribution for a CMP bin in the study area. Note that an even distribution is reached if we used no more than 6,000 m offset.

CHAPTER 6

RESULTS AND VALIDATION

In this chapter, the results from anisotropy analysis are presented and compared with curvature and coherence in Unayzah-C reservoir and with image logs and well test data in Unayzah-A reservoir.

6.1 Results

Anisotropy azimuth and intensity are presented as color-coded maps in Figure 6.1 for Unayzah-C reservoir. The long axis of the anisotropy ellipse is displayed on a structural contour map for Unayzah-C reservoir in Figure 6.2 for all ellipses and for only the highest anisotropy intensity (values greater than 1). The same maps are displayed in Figures 6.3 and 6.4 for Unayzah-A reservoir. The maximum ellipticity (anisotropy intensity) ratio is 4.21 (421%) for Unayzah-C reservoir and it is 3.97 (397%) for Unayzah-A reservoir. Curvature and coherence attributes were also extracted for both Unayzah-C and Unayzah-A reservoirs for comparison and validation purposes (Figure 6.5).

In both Unayzah-C and Unayzah-A reservoirs the highest anisotropy intensity is located along the relatively steeper western flank of the field structure. Orientation of the ellipses looks very chaotic in both reservoirs. A key question to answer is how well the anisotropy captures the actual fracture density and orientation from well data. For this

purpose we examine the fracture relevant data first and then compare the results from AVOA analysis with well data in Unayzah-A, after that we compare curvature and coherence attributes with AVOA analysis in Unayzah-C reservoir.

6.2 Timing and Types of Fracturing and Faulting

Only one or two image logs cover some section of Unayzah-C reservoir, and no fractures could be identified. Image log coverage and almost all the fractures detected are in Unayzah-A reservoir. Most of the fractures encountered in image logs are nonconductive (Figure 6.6). They are most probably cemented fractures but some could also be granulation seams, which are common in clastic sediments. Granulation seams are actually fractures that are filled with sand and clay gouge and have lower permeability than in the matrix. There are also a small number of conductive layer bound fractures (Figure 6.7). The cemented fractures may belong to the early Paleozoic or Cretaceous deformation pulses and the open fractures belong to the Late Tertiary Zagros orogeny.

A reverse fault was interpreted within Unayzah-A reservoir in WELL-K (Figure 6.8). Total losses were encountered in WELL-L within Jilh and a reverse fault was inferred which extends down to Unayzah-C reservoir. The presence of reverse faults on the steep western flank and the westward asymmetry of the field structure suggest a compressional deformation during Paleozoic when the structure was first formed. It is also possible that compression and reverse faulting was reactivated during the Late Cretaceous NW-SE Oman compression.

6.3 Fractures from Borehole Images

Image logs are available only from vertical wells and very few fractures are encountered in these logs. There are a total of 23 fractures in 7 wells (Figure 6.9). Two of the wells have no fractures at all. A total of 13 fractures are nonconductive. Only 10 conductive fractures are present and these are actually very small layer bound fractures in only two wells (WELL-L and WELL-H). Fractures in WELL-A are not included since the few fractures intersected are within carbonate reservoirs far above the Unayzah-A reservoir. Even so only 13 very small fractures are picked in this well.

The overall strike of conductive fractures is NE-SW and of nonconductive fractures is N-S. Although fractures strike NE-SW and NW-SE in WELL-K, the small reverse fault is oriented NNW, parallel to the steep flank of the structure supporting the hypothesis that the western flank is faulted.

6.4 Fractures from Well Testing

Out of eight wells with well testing, only WELL-I intersects a fracture zone or small conductive fault. All the remaining seven wells are interpreted as homogeneous matrix wells, which means there cannot be any fracturing or fracture corridors within the radius of investigation of these wells (Figure 6.10).

6.5 Fractures and Fault Overview

No total losses were reported in wells within the Unayzah formation. The latest simulation runs achieved a good history match without any fractures and faults within Unayzah-A reservoir. The image logs, losses and well testing suggested possible faulting on the steep western flank of the field (WELL-K and WELL-L). The only other well with fracture intersection away from the steep western flank was well WELL-I on the eastern flank. The overall impression is that the Unayzah-A reservoir is not a fractured reservoir. This may be attributed mainly to the friable nature of the eolian sands. Borehole stability reports indicate sand flow, which means the sand is not well cemented and hence difficult to fracture. The mild structural relief could also be an additional explanation why the reservoirs in the field are not fractured. Compared to nearby Ghawar, this field is a very low-lying flat structure.

It is difficult to assess the degree of fracturing of Unayzah-C reservoir but the overall structural configuration of the field and the heterogeneous nature of the reservoir also suggest the Unayzah-C may also be devoid of fractures, except perhaps along the faulted steep western flank.

One additional drawback for seismic fracture detection is the dominance of nonconductive fractures. Even if the Unayzah-C reservoir was highly fractured, it would be difficult to detect the fractures from anisotropy if the fractures are mostly cemented or filled with sand-clay gouge.

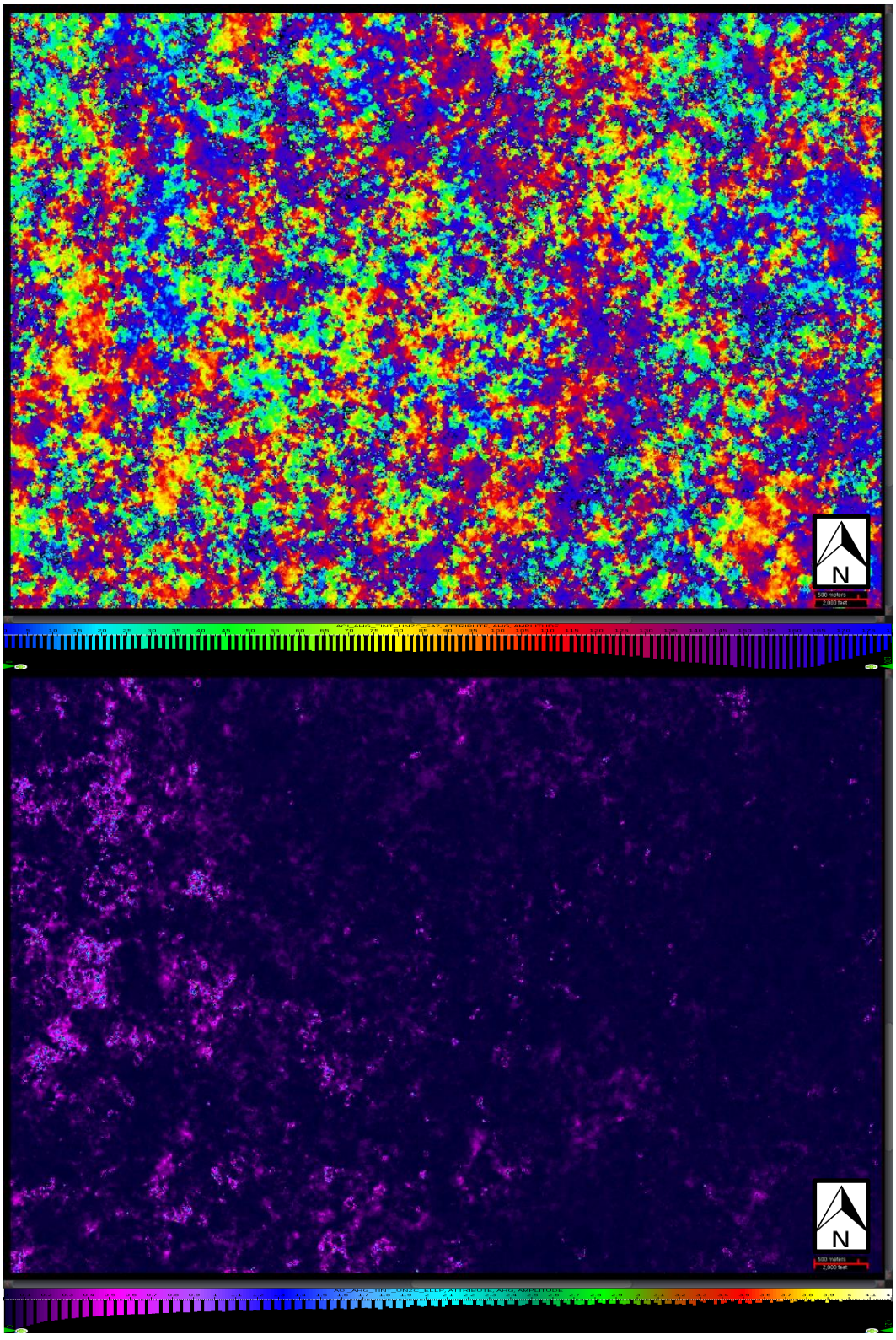

Figure 6-1- Unayzah-C anisotropy azimuth (top) and intensity (bottom) maps.

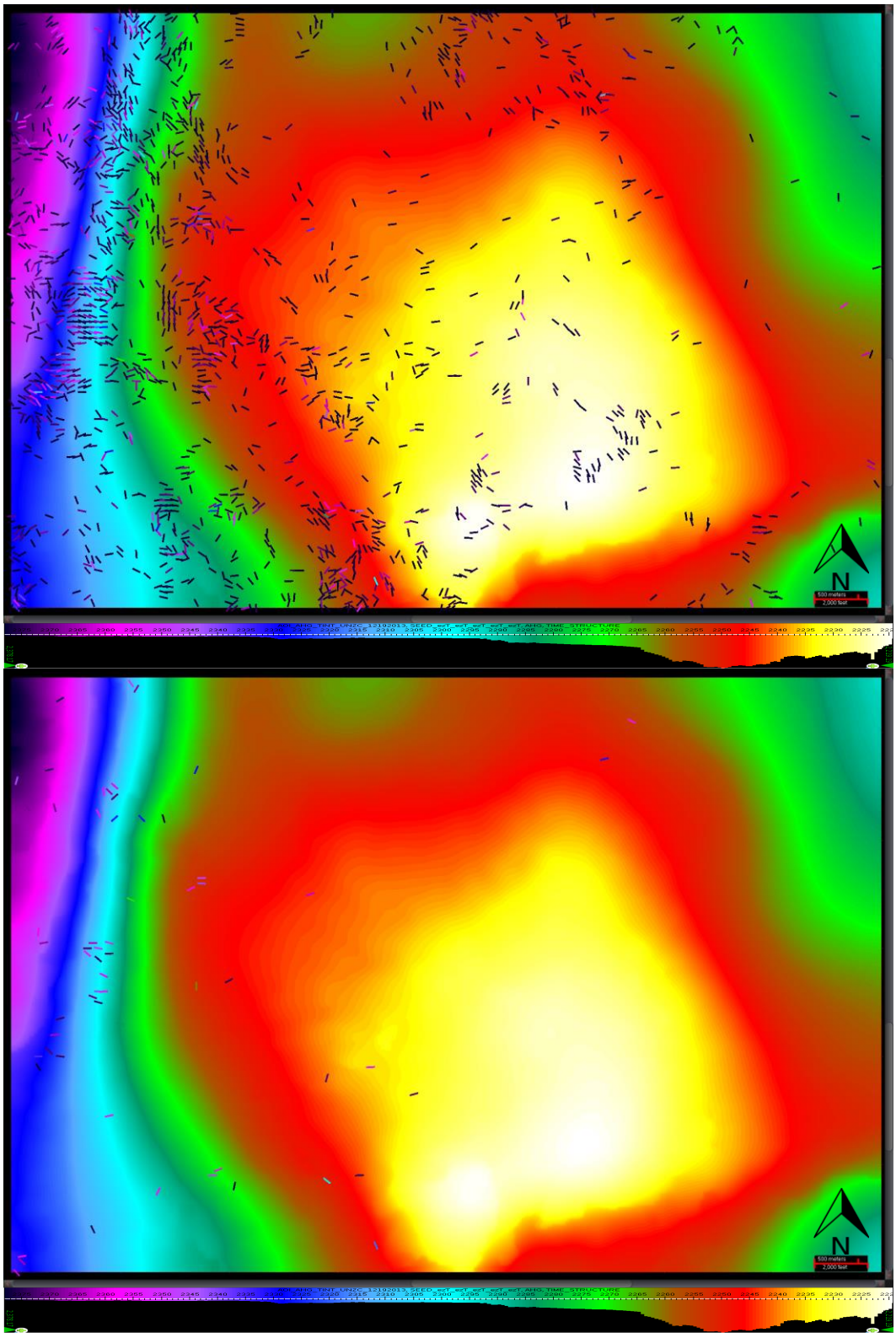

Figure 6-2 - Unayzah-C display of long axis of anisotropy ellipses on structural contour map. The lower map shows only the sticks with the E values greater than 1.

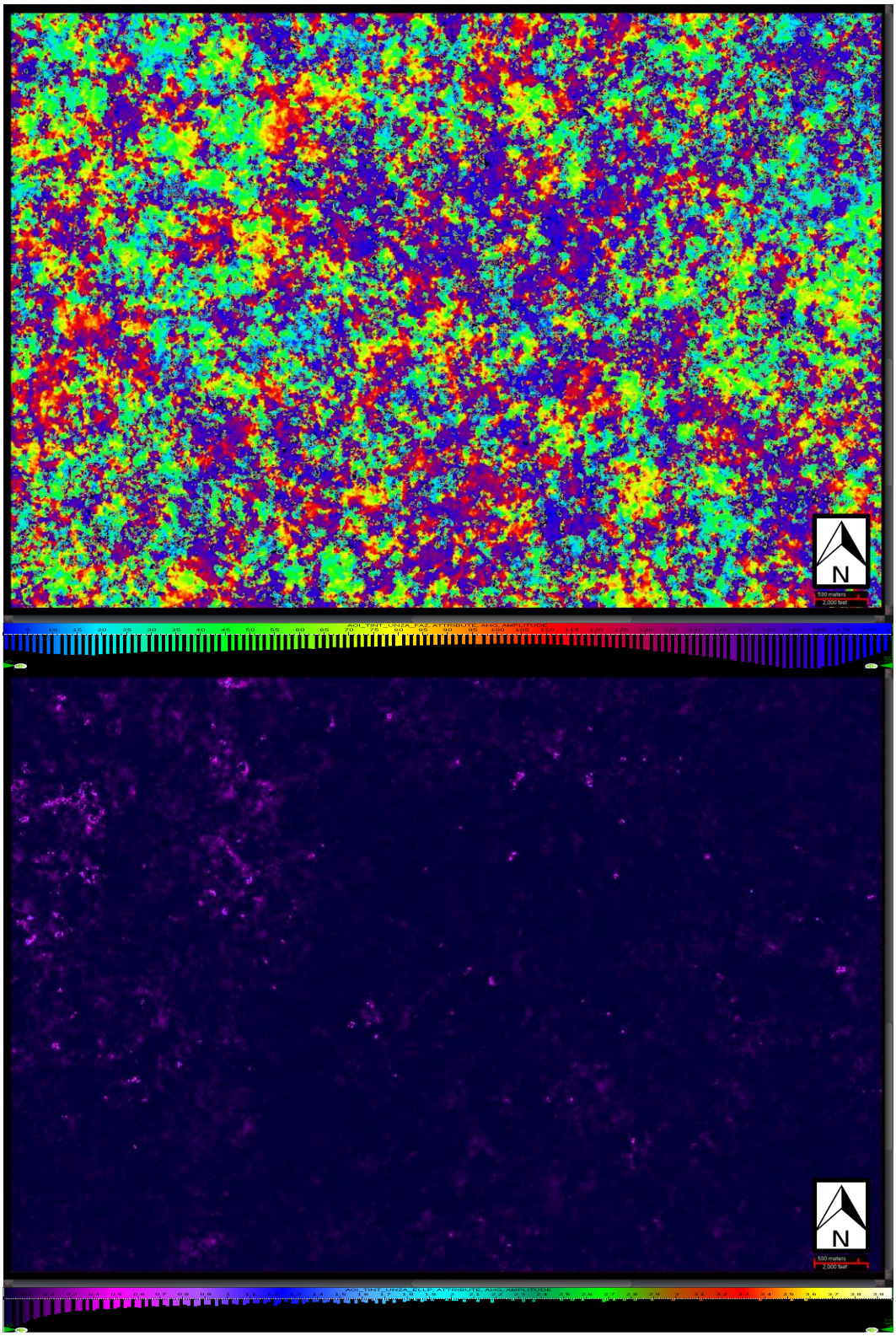

Figure 6-3 - Unayzah-A anisotropy azimuth (top) and intensity (bottom) maps.

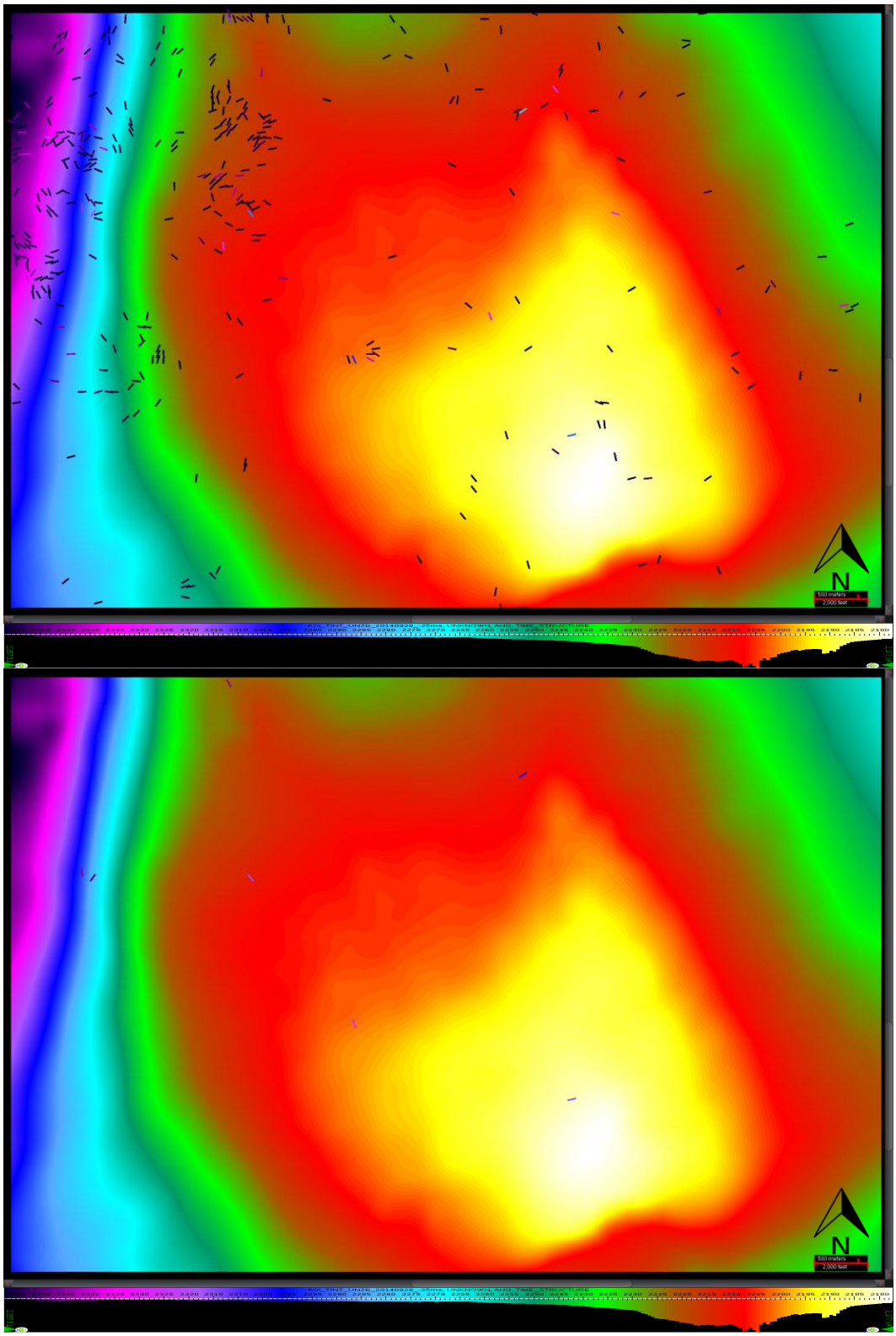

Figure 6-4 - Unayzah-A display of long axis of anisotropy ellipses on structural contour map. The lower map shows only the sticks with the E values greater than 1.

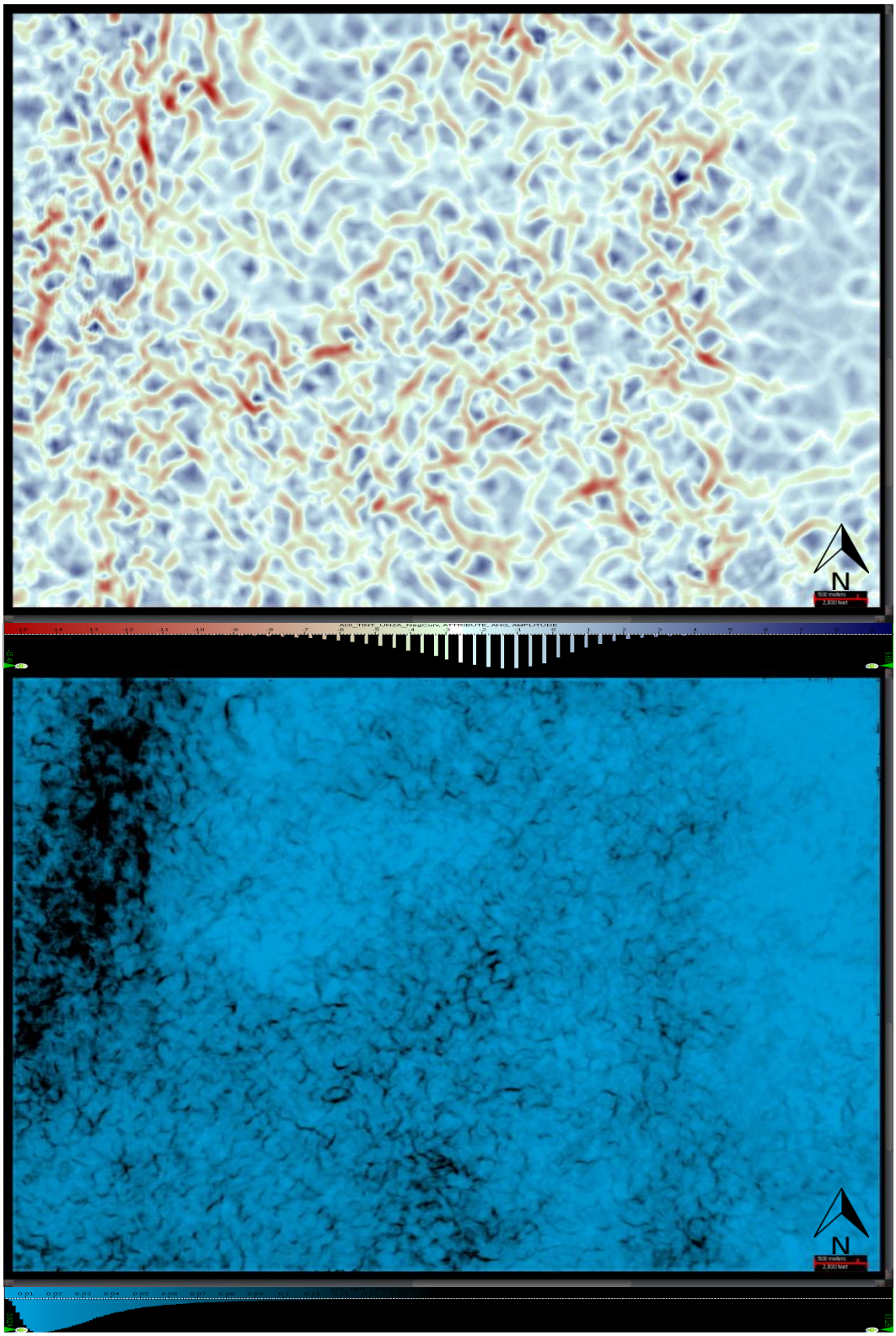

Figure 6-5 - Examples of curvature (top) and coherence (bottom) maps (Unayzah-A).

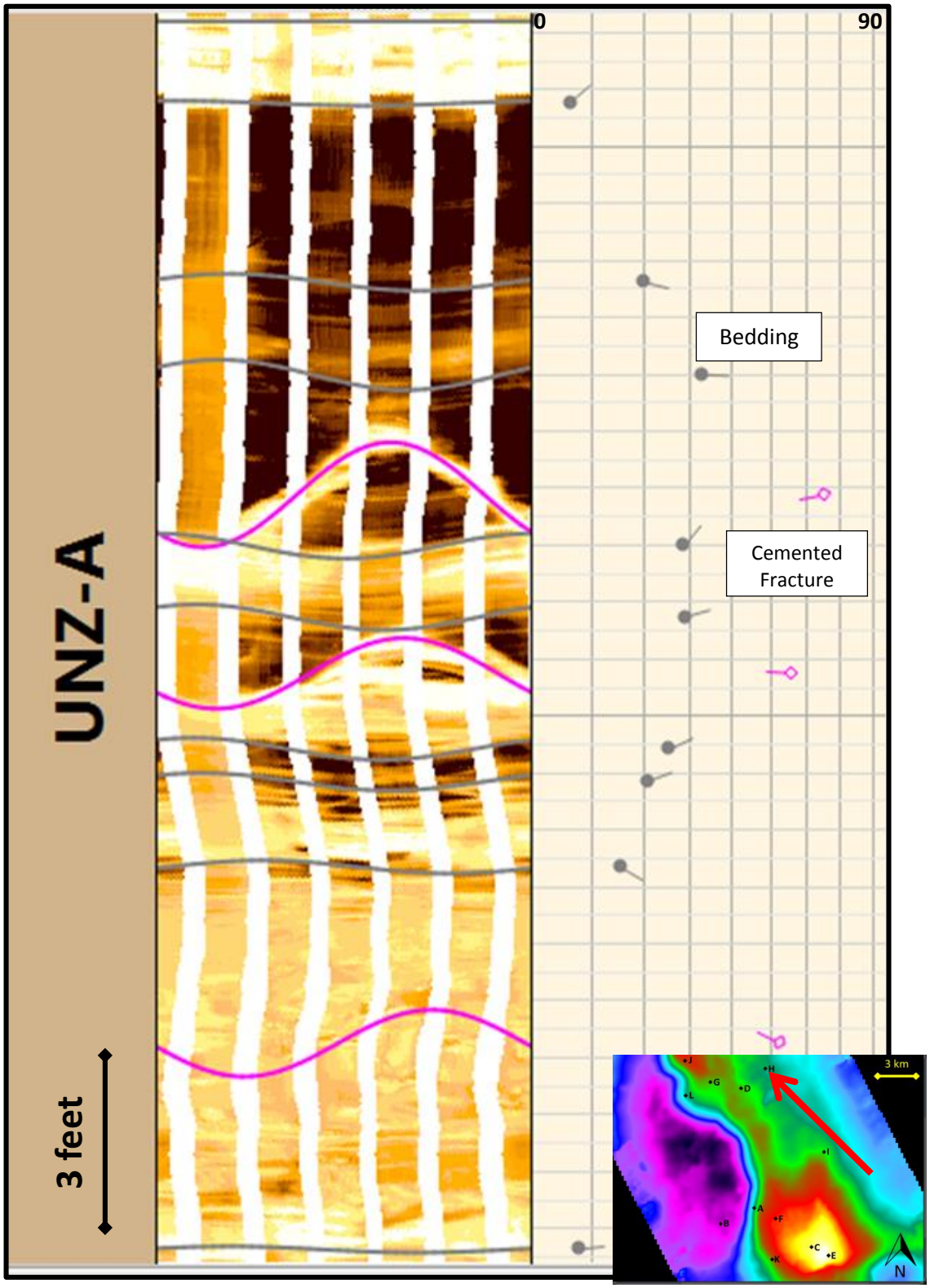

Figure 6-6 - Nonconductive fractures in Unayzah-A in WELL-H. Gray tadpoles represent bedding and pink tadpoles represent cemented fracture.

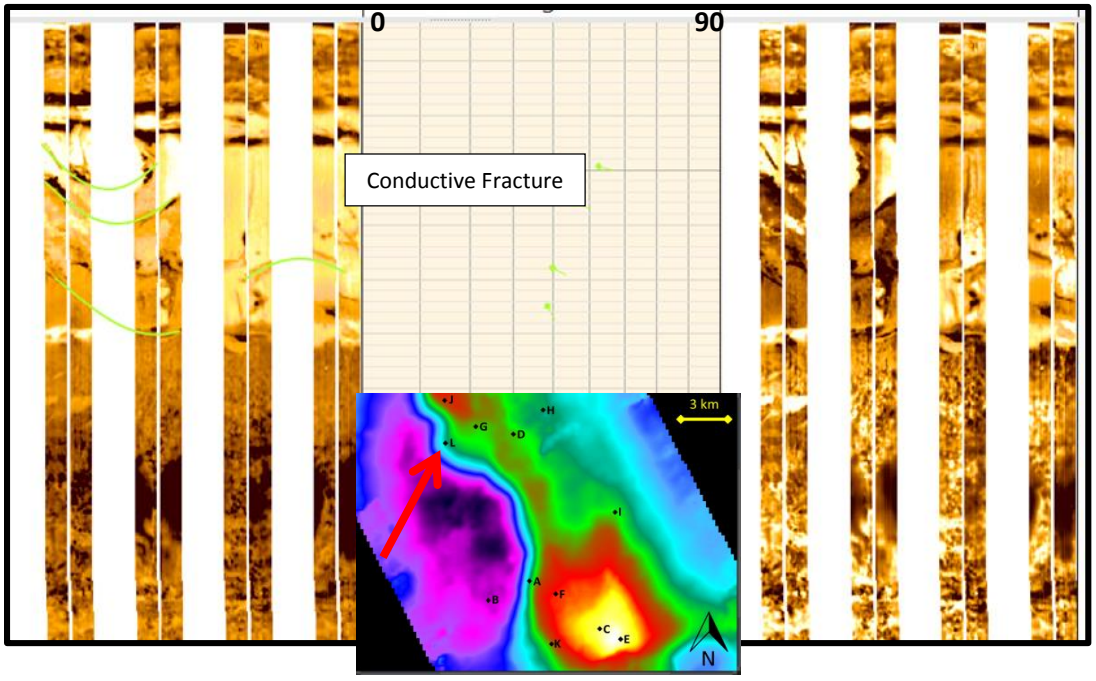

Figure 6-7- Few layer-bound conductive fractures in Unayzah-A WELL-L. Green tadpoles represent conductive fracture.

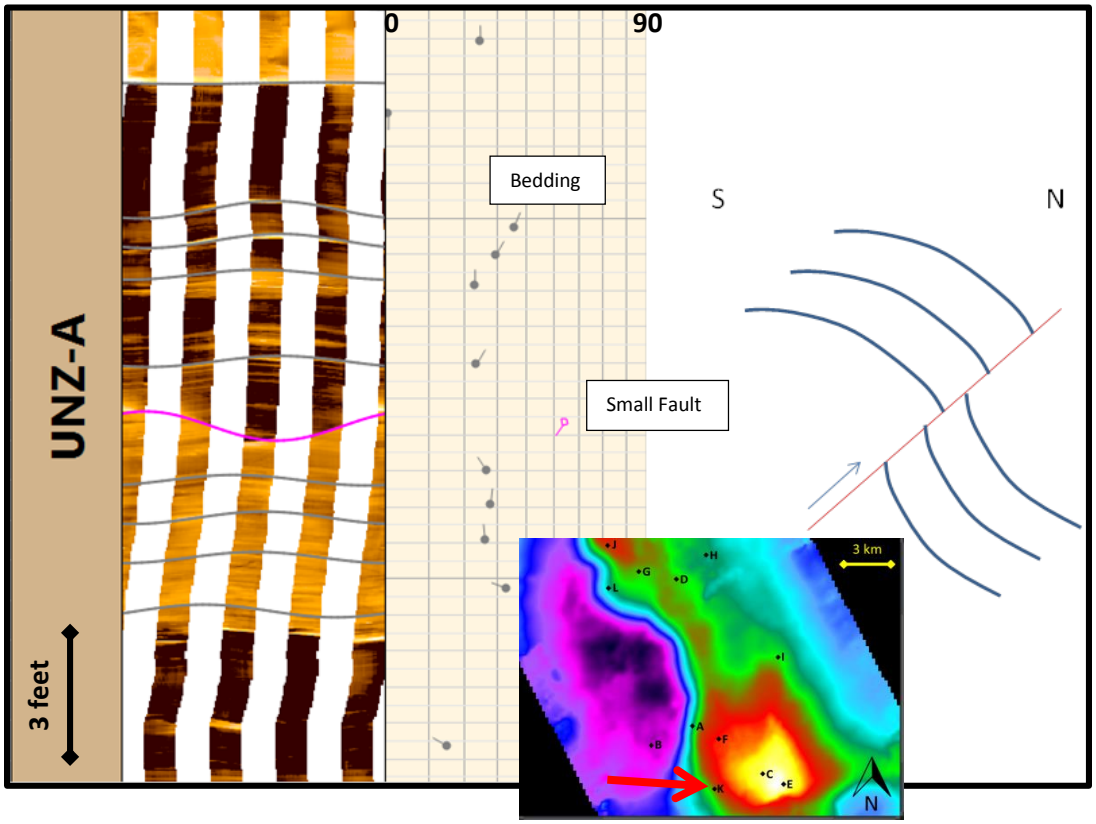

Figure 6-8 - A nonconductive reverse fault within Unayzah-A in WELL-K. Gray tadpoles represent bedding and pink tadpole represents small fault.

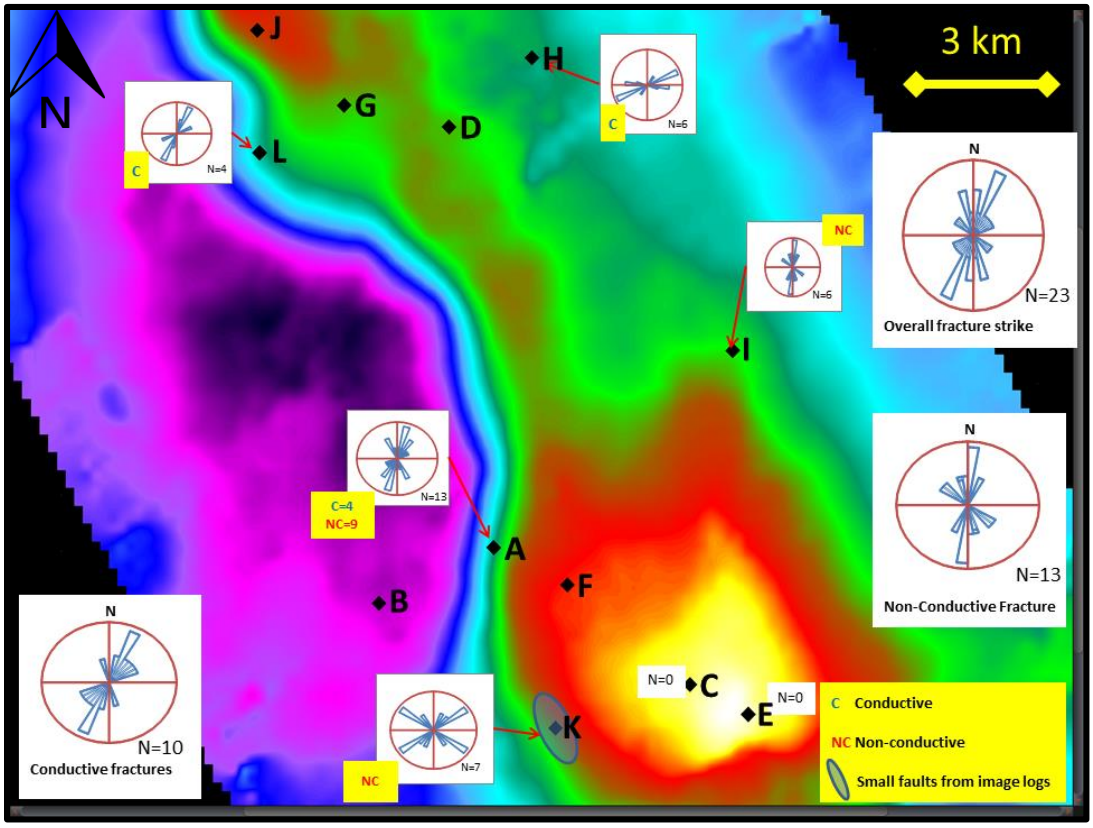

Figure 6-9 - Fracture azimuths from borehole image logs in Unayzah-A

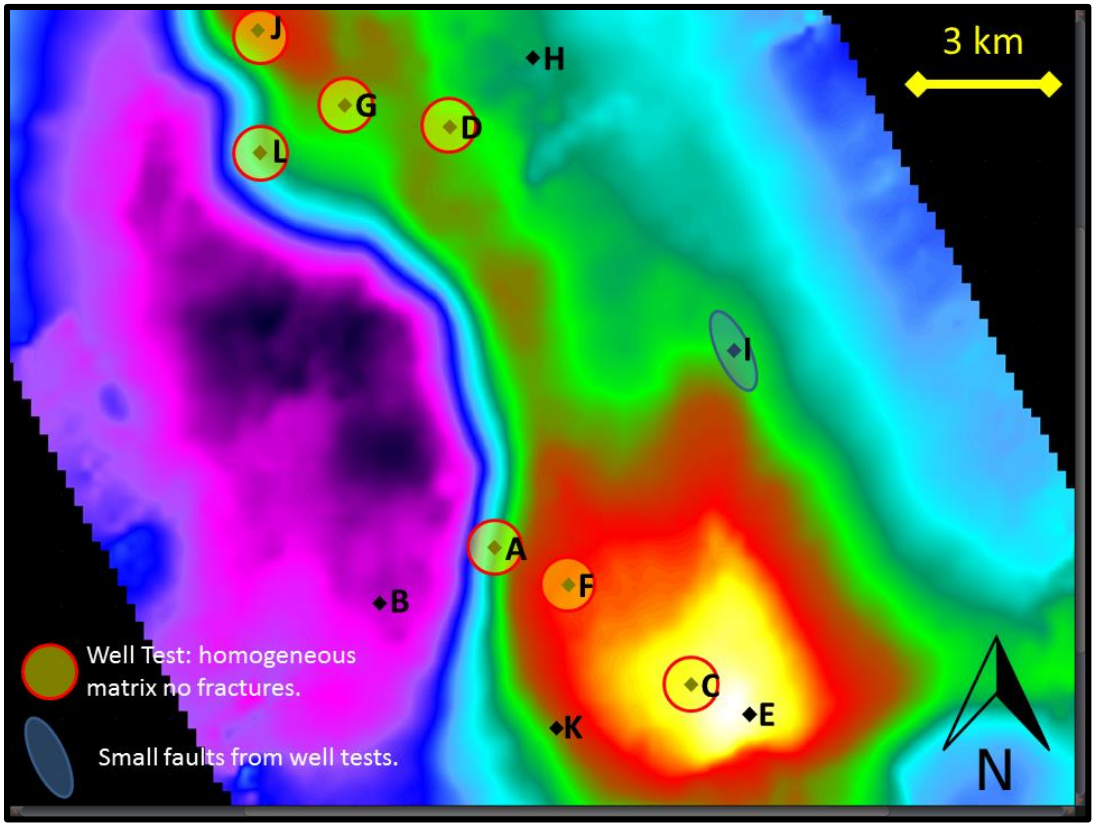

Figure 6-10 - Fractures and exclusion zones from well testing.

6.6 Regional In-Situ Stress and Critically Stressed Fractures

Drilling induced fractures from various wells consistently has a NE-SW strike (Figure 6.11). Similarly, breakouts are oriented in NW-SE direction (Figure 6.12). Both breakouts and drilling induced fractures indicate a NE-SW maximum in-situ stress (Figure 6.13). A total of 197 induced fractures and 14 breakouts are measured. The in-situ stress orientation from borehole image logs of the Unayzah-A wells is consistent with the in-situ stress orientation derived by GeoMechanics International (GMI) in Tuwaiq Mountain formation in the region (GMI, 2010). GMI also compiled data on the magnitudes of the present day in-situ stresses. Accordingly in the WELL-A:

Vertical stress is S_v = 153.2 lb/ft^3.

Maximum horizontal stress is S_{hmax} = 206.7 lb/ft^3.

Minimum horizontal stress is S_{hmin} = 134.6 lb/ft^3.

Pore pressure is Pp = 91.0 lb/ft^3.

With these data, the field falls within a strike slip tectonic regime (Ozkaya, personal communication).

Present-day in-situ stress is important for two reasons. First, fractures that are nearly parallel to maximum horizontal in-situ stress are more likely to be fluid conductive. The second reason is the connection between seismic anisotropy and in-situ stress. In the absence of any fractures, difference in maximum and minimum horizontal stress may create seismic anisotropy because of micro cracks that form parallel to maximum in-situ stress.

A GMI study in different reservoirs and wells including WELL-A, WELL-B, WELL-L, WELL-G and WELL-J failed to show existence of any critically stressed fractures in the area (Figure 6.14). This means fluid conductive fractures, which are the focus of interest, are unlikely in this field. This in a way supports the conclusion pointed by production data, simulation, well tests and available borehole image logs. Since WELL-A and WELL-B are on the steep western flank where faults are supposed to exist, the conclusion by GMI is discouraging because conductive fractures are not expected even within the potentially faulted northern flank of the field.

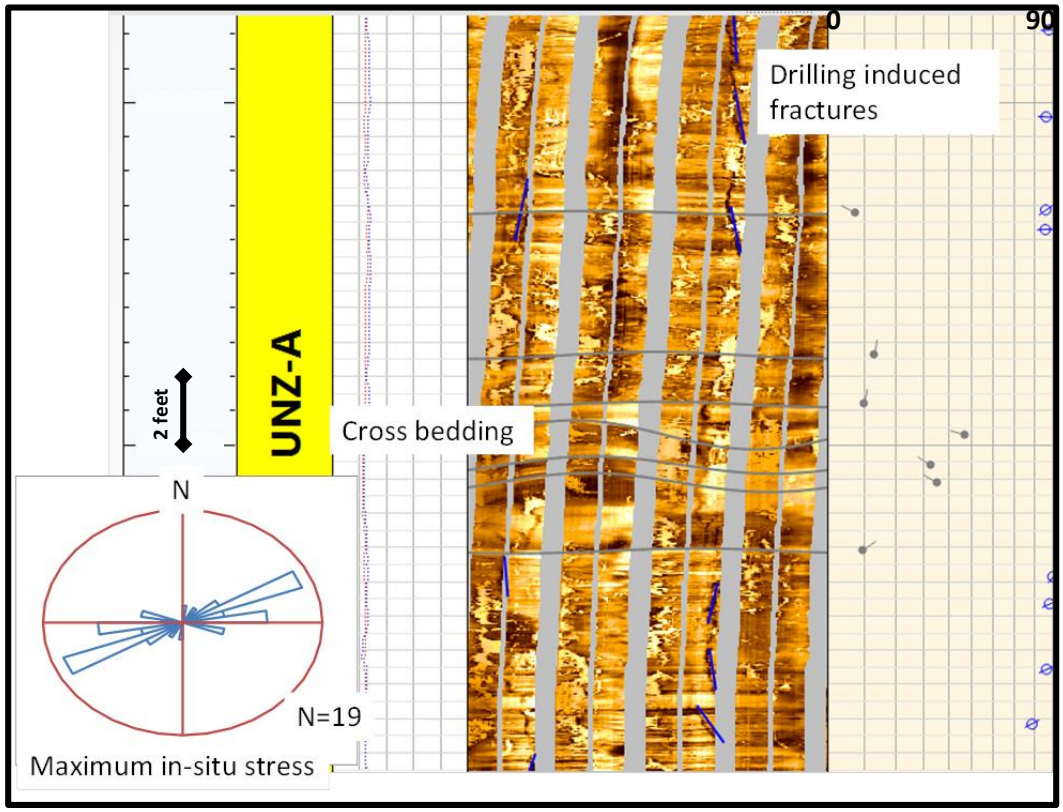

Figure 6-11 - Drilling induced fractures. Gray tadpoles represent cross bedding and blue mark represent drilling induced fractures.

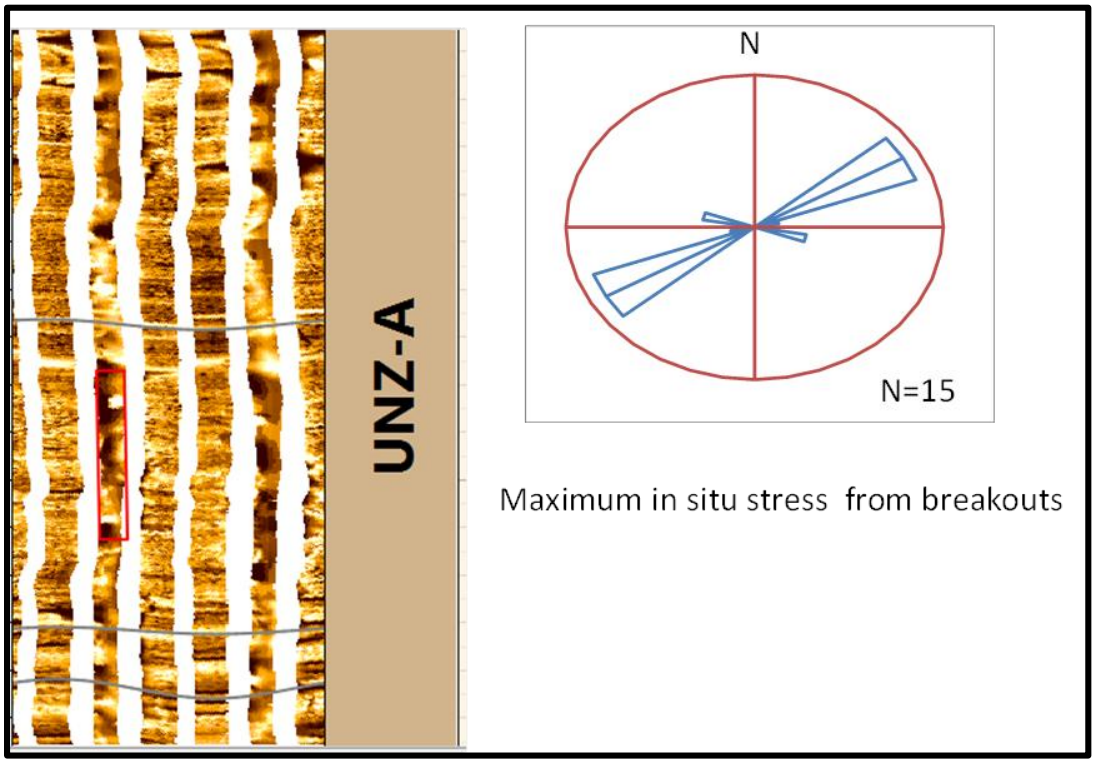

Figure 6-12 - Breakout example.

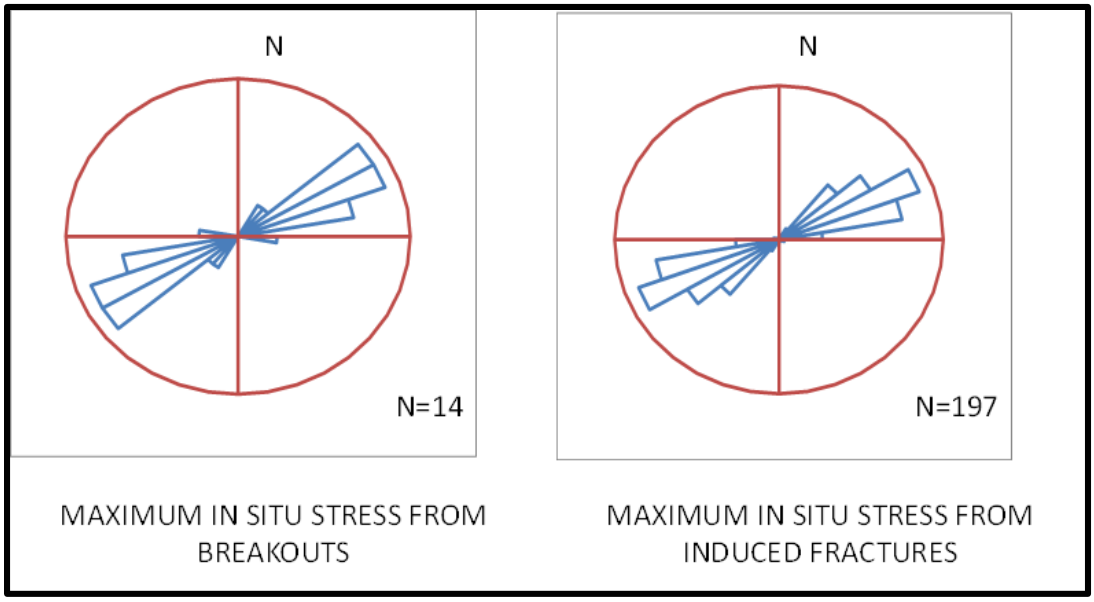

Figure 6-13 - Maximum in situ stress direction from breakouts and induced fractures.

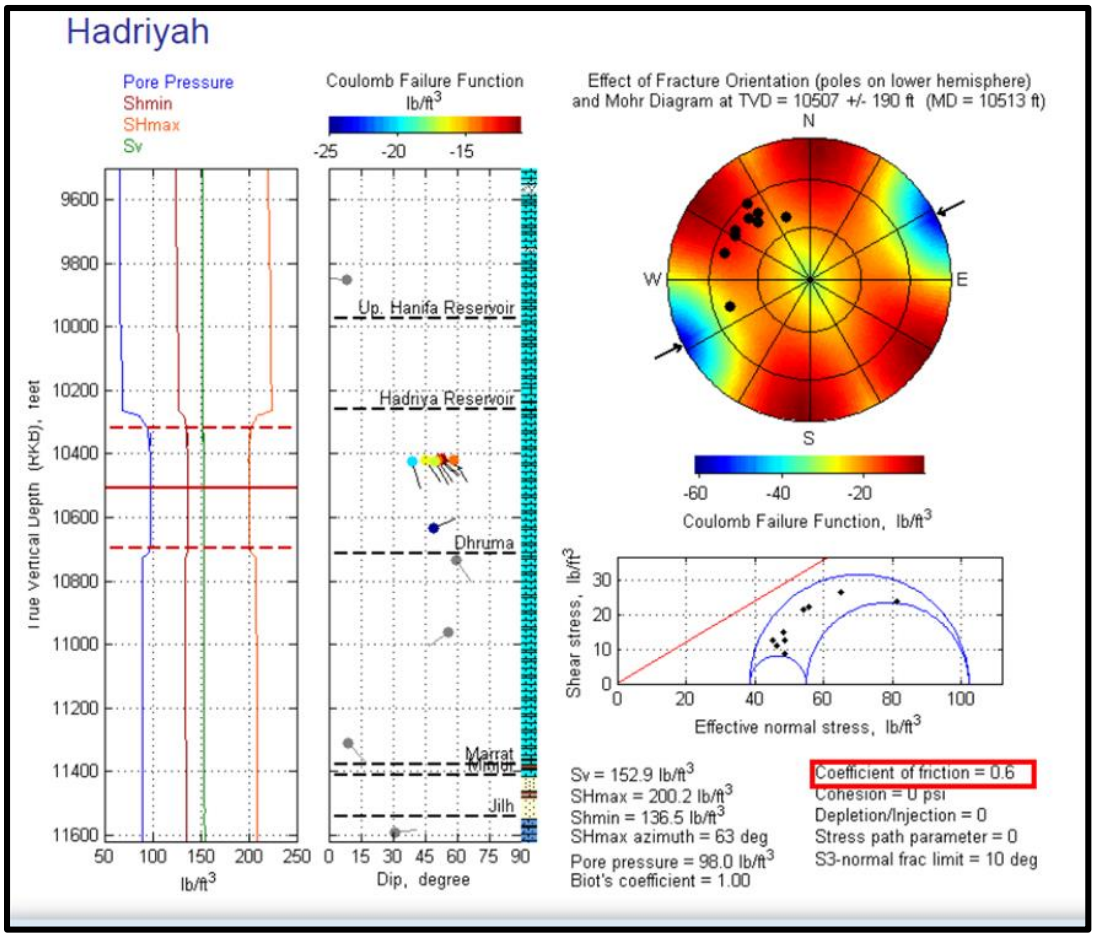

Figure 6-14 - Stress values and analysis of critically stressed fractures (GMI, 2010).

6.7 Comparison of Fractures from Well Data and AVOA

A combination of borehole image logs and well test data suggests there are only very sparse conductive fractures in the field within Unayzah-A reservoir and these fractures strike NE-SW. There are two or three cemented faults/fracture zones; two of which are located within the relatively steep western flank of the field structure (Figure 6.15). These faults/fracture corridors strike nearly N-S parallel to the structural trend on the western flank. Unfortunately, neither the intensity nor the orientation and distribution of AVOA anisotropy ellipses reflect the fracture data from well data. The field is almost devoid of conductive fractures as indicated by well testing, image logs, and simulation results. For the limited number of conductive fractures, fracture strike from well data has no agreement with strike of maximum anisotropy direction from seismic data.

Although there is some agreement with the concentration of high anisotropy on the west flank of the structure, the orientation of the ellipses is NW-SE, not in alignment with the N-S trend of structures and small nonconductive faults.

6.8 Comparison of Anisotropy with Other Seismic Fracture Indicators

No borehole image logs or dynamic data are available within Unayzah-C reservoir to enable comparison of anisotropy with well data. It was therefore decided to generate curvature and coherence maps and compare the results with anisotropy. Coherence and

curvature maps were also prepared for Unayzah-A reservoir to see how these attributes correlate with well data.

There was no visual or statistical correlation between ellipticity, curvature and coherence (Figure 6.16 and 6.17). Although there seemed to be some visual correlation between curvature and coherence, no statistical correlation was found.

Both curvature and coherence maps from Unayzah-A reservoir look very similar to those from Unayzah-C reservoir (Figure 6.18 and 6.19). Neither the curvature nor the coherence maps have any correlation to borehole image data from well data that suggests very sparse or no fracturing in the field within Unayzah-A reservoir.

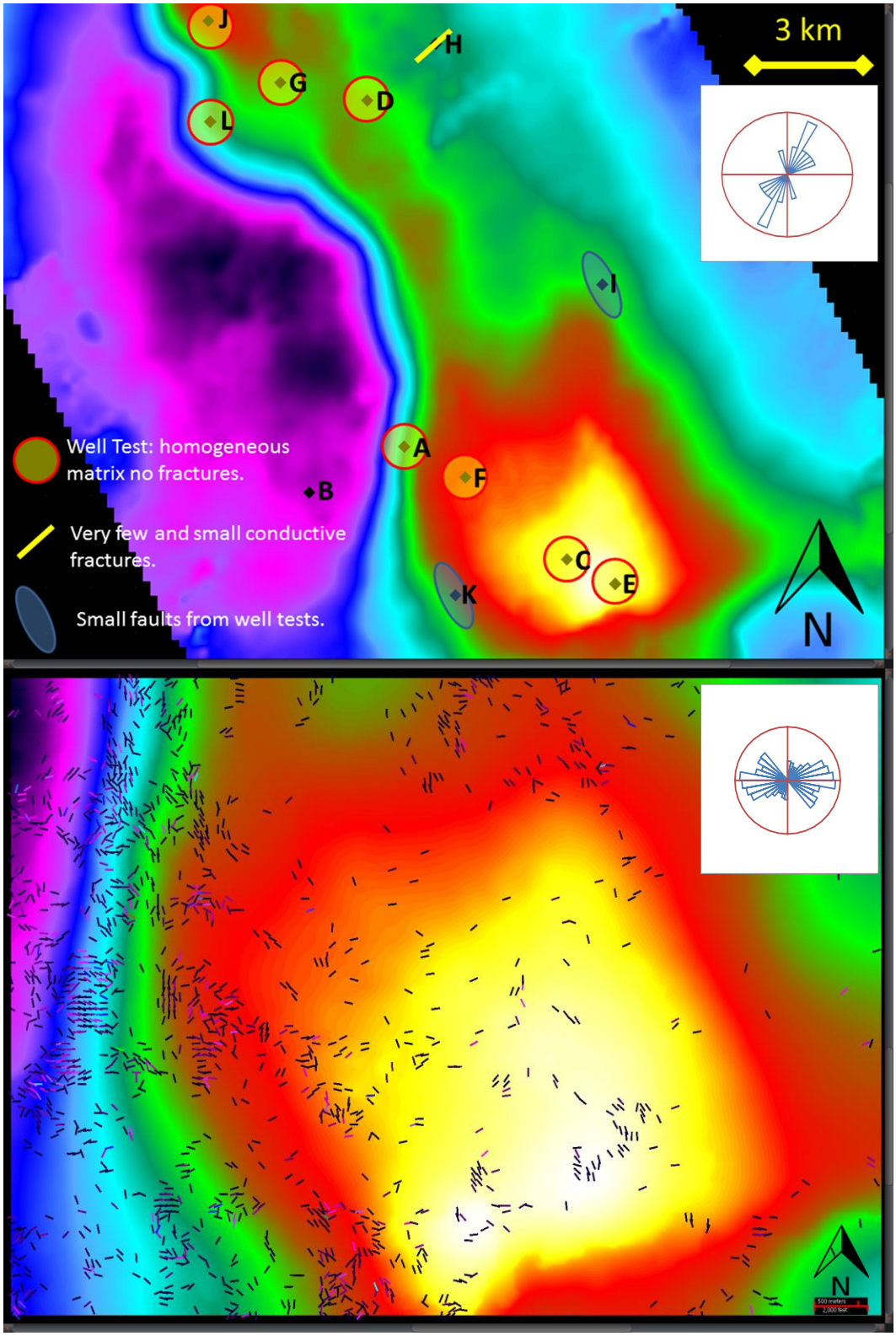

Figure 6-15 - Comparison of fracture data from wells (top) and AVO (bottom). The lower map shows only the southern lobe of the field structure. The rose diagram at the top shows the strike of conductive fractures from borehole images.

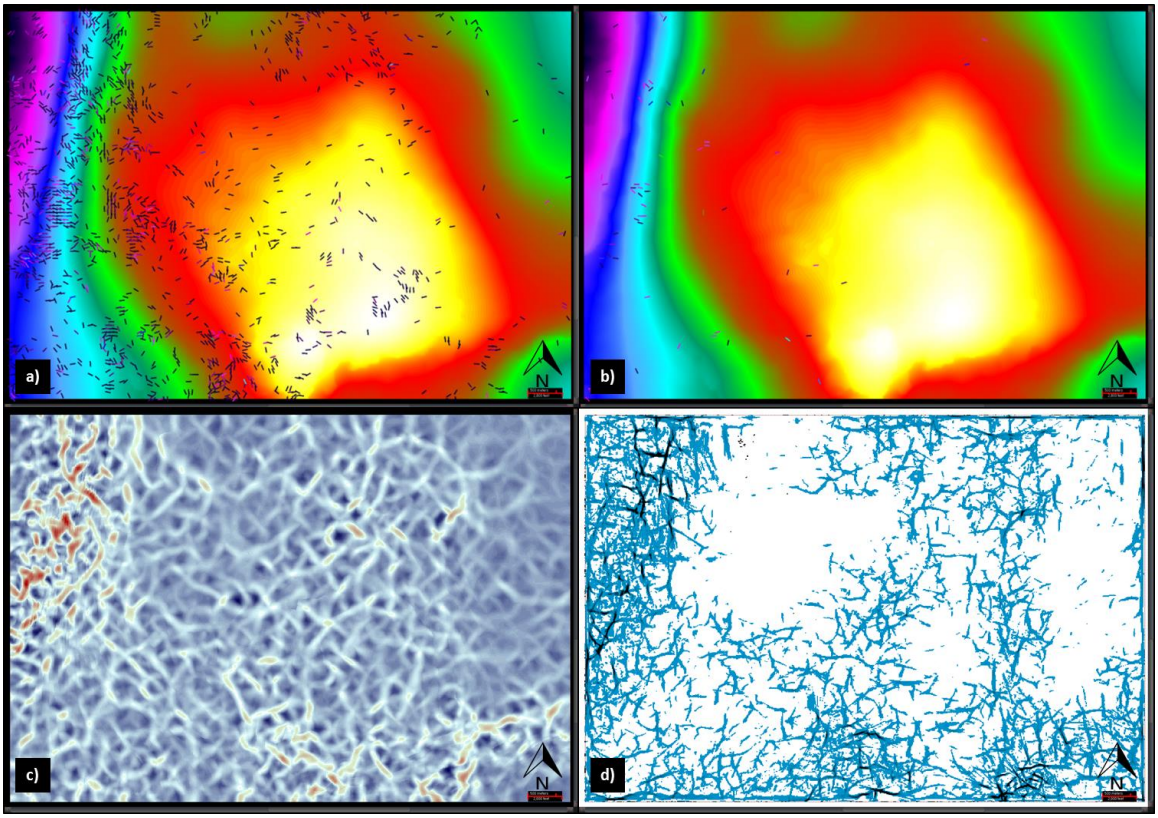

Figure 6-16 - Comparison between a) AVOA ellipticity b) AVOA ellipticity with values greater than 1, c) curvature and d) coherence maps.

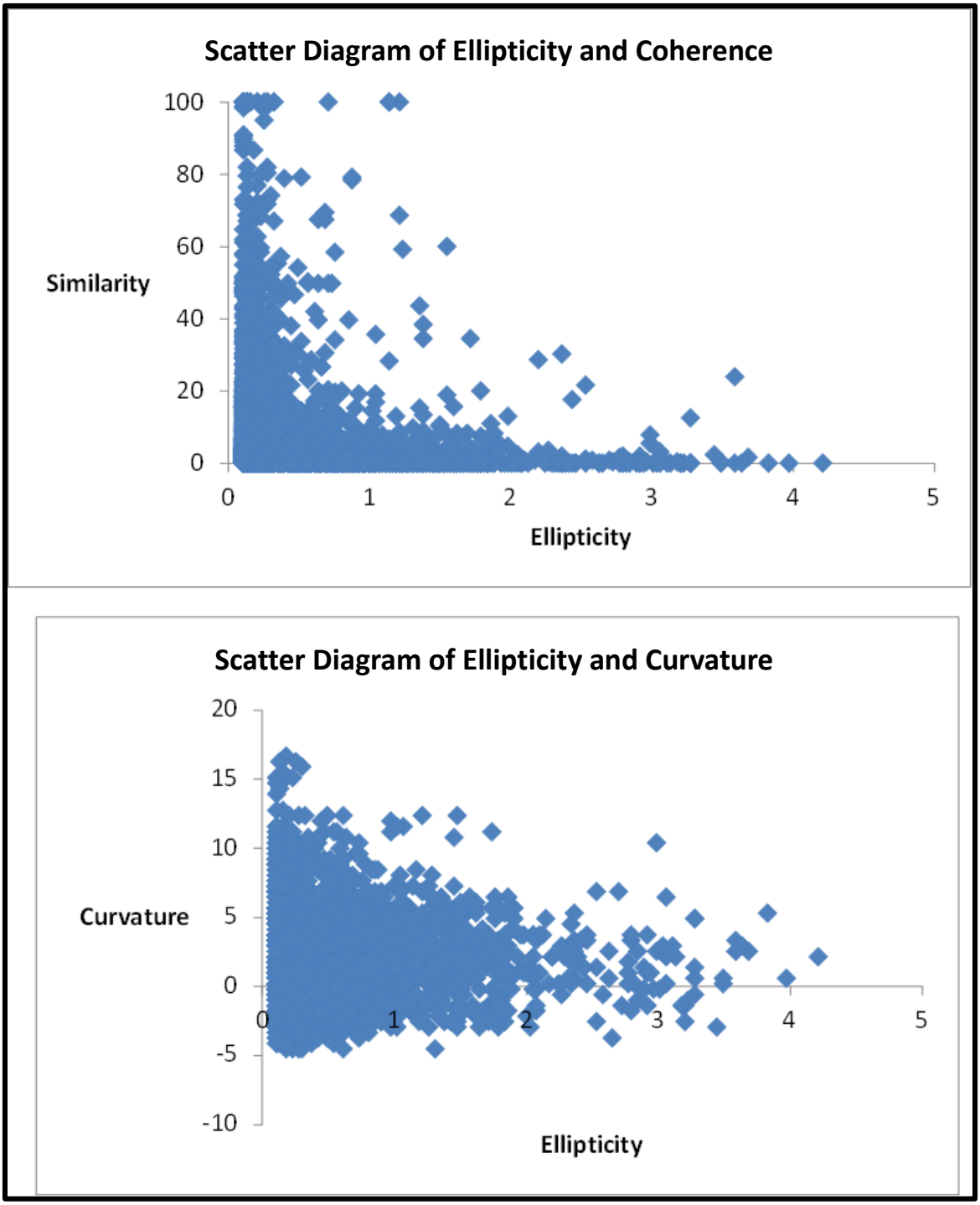

Figure 6-17 - Scatter diagrams between ellipticity, curvature and coherence.

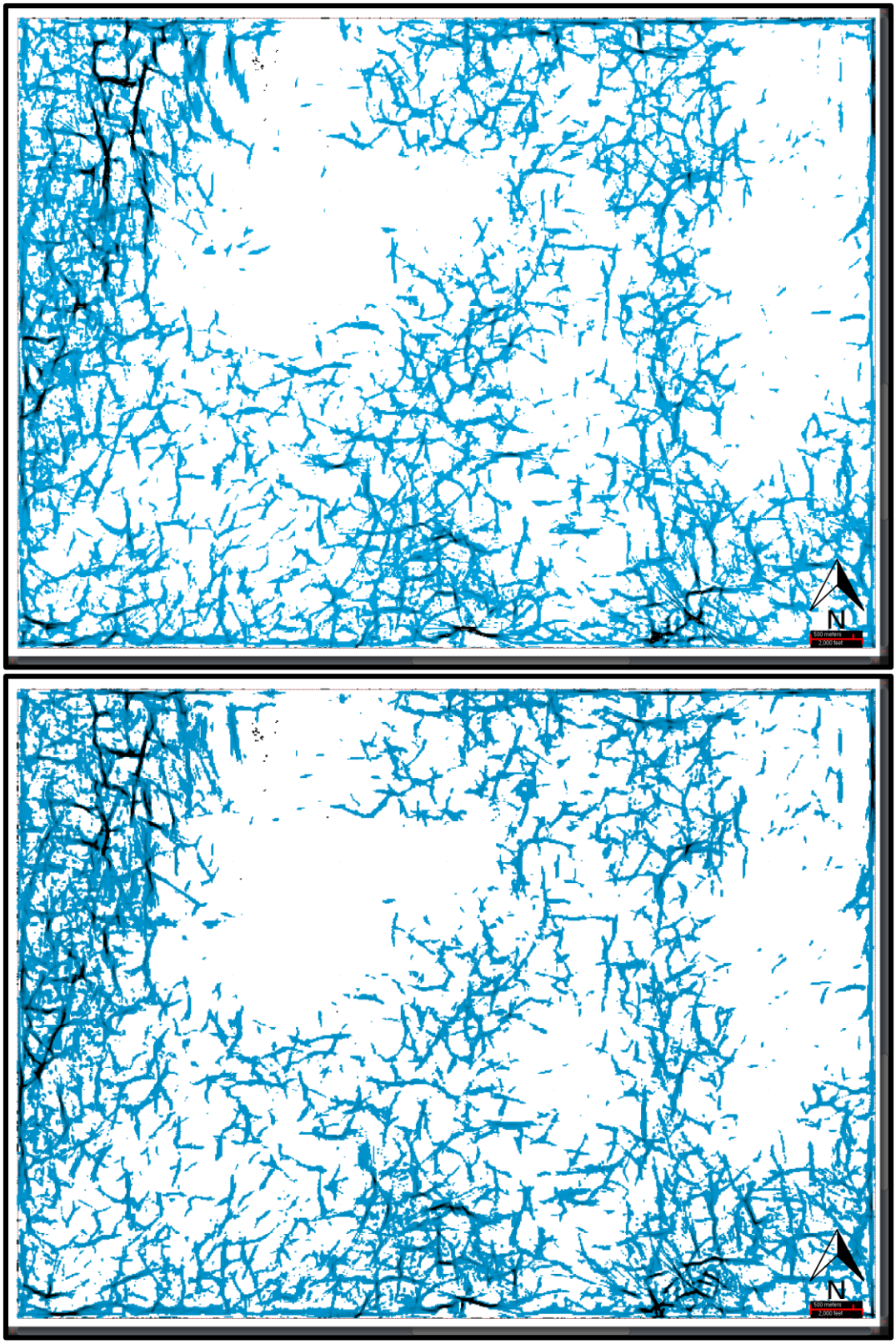

Figure 6-18 - Coherence maps of Unayzah-A (above) and Unayzah-C (below).

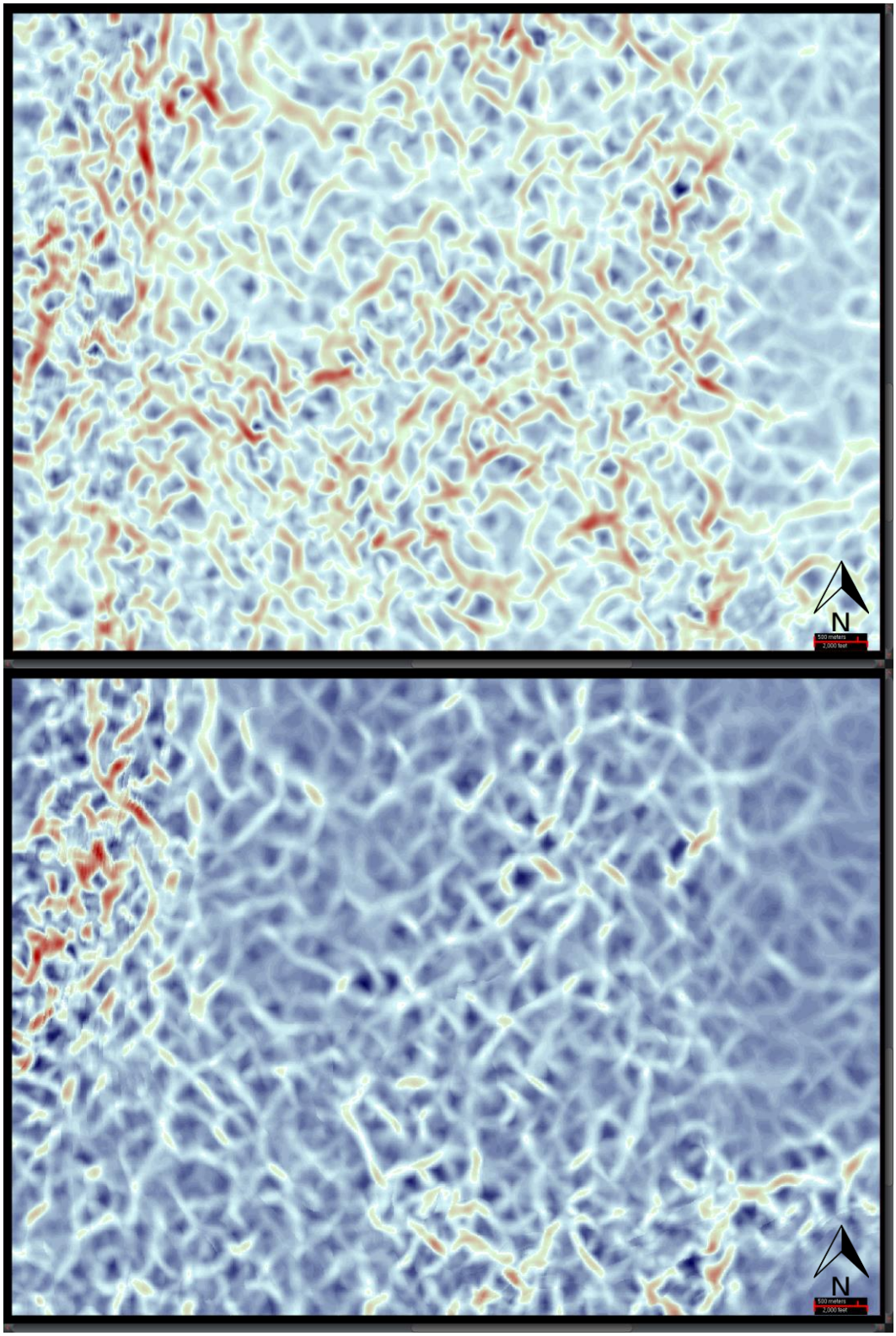

Figure 6-19 - Curvature maps of Unayzah-A (above) and Unayzah-C (below).

CHAPTER 7

CONCLUSION AND DISCUSSION

Delineating and characterizing fractures within the clastic reservoirs, Unayzah-C and Unayzah-A reservoirs, in Eastern Central Saudi Arabia is a challenging task to geoscientists. AVOA method was implemented on 3D full-azimuth broadband seismic data over a study area. The results were validated with available well data such as borehole images, well testing and production data in the Unayzah-A. For Unayzah-C, there were no borehole images or production data to validate the results. For that reason, curvature and coherence were used as alternative seismic fracture detection methods.

The AVOA ellipticity maps portray both Unayzah-C and Unayzah-A reservoirs as highly fractured reservoirs. Although the orientation and distribution are different, both curvature and coherence attributes also predict fractured reservoirs. The well data, production data, and simulation results show the opposite for Unayzah-A reservoir. The AVOA technique has been successfully applied in many fields around the world (e.g., Lee et al., 2010; Gray, 2000; and Sun et al., 2012). There are also few papers on fracture detection by AVOA in Saudi Arabia (Neves et al., 2003; Al Hawas et al., 2003; Balhareth, 2009; Burnstad and Keho, 2011). It is important to understand why the AVOA method was not very successful in this particular case. Below we will first survey shortcomings of the method in general and uncertainties particular to the Unayzah reservoirs in the study area.

AVOA is an umbrella of various slightly or very different techniques and methods. The only common aspect of all is their starting point: usage of velocity or amplitude anisotropy. Different techniques have different advantages and disadvantages. The literature is full of papers each advocating a particular approach or how variation in some aspects of analysis improves fracture detection. Sayers (2007) presents an overview of AVOA shortcomings, which include stumbling blocks such as multiple fracture sets, difference between in-situ stress orientation and dominant fracture strike, fracture compliance and gas saturation. Sayers (2007) emphasizes that "… constraints from logs, borehole images, and production data are essential in interpreting measurements on fractured reservoirs …"

Among the complications not mentioned by Sayers (2007), I may add the effect of overburden anisotropy (Liu et al., 2011), heterogeneity of the formations and disagreement between velocity anisotropy and amplitude attenuation (Liu et al., 2007). Sen et al. (2007) showed a case study where AVOA signature does not show the variation expected from the Cadotte formation in the Lynx field, Alberta, Canada. They suggested that the reason for such a behavior could be the tuning effect. The deep Falher formation shows an unexpected large AVOA signature that could have been transmitted from the upper Cadotte formation. The effects of transmission through an anisotropic overburden are generally ignored. Jenner (2001) concluded that the results from AVOA and azimuthal velocity analysis are not the same due to the impact of different characteristics of the subsurface geology. The AVOA has higher vertical resolution and is more sensitive to rock properties across the reservoir. The azimuthal velocity variation is affected by the bulk rock properties over a more localized vertical and horizontal extent.

The striking aspect of the current study is the disagreement between AVOA or curvature and coherence and well data. Seismic data indicates an abundance of fracture lineaments, but both borehole images and production data do not support this finding in Unayzah-A reservoir, which according to production data and image logs, is an essentially clastic reservoir with only few small conductive fractures. A similar abundant fracturing is conveyed from seismic data in Unayzah-C reservoir. In this case, there is no production or image data to counter or support seismic fractures. Curvature and coherence attributes in both Unayzah-A and Unayzah-C reservoirs cast doubt on the validity of the fractures detected by seismic analyses especially if one remembers that Unayzah-C reservoir is an extremely heterogeneous glacial clastic deposit.

One possible explanation that can be offered is the weakness of anisotropy in the Unayzah clastic reservoirs. The maximum ellipticity (anisotropy intensity) ratio is 4.21 (421%) for Unayzah-C reservoir and it is 3.97 (397%) for Unayzah-A reservoir. Most values are less than 1 (weak anisotropy). Values greater than 1 are few and are confined to the steep western flank where few faults have been documented by image logs and loss of circulation and where coherence and curvature indicate some faulting. If the values less than 1 are eliminated (assuming it is related to background noise from seismic) then the method is in agreement with well data in the sense that there is no major fracturing in the field within the Unayzah-C and Unayzah-A reservoirs. It is likely that in most locations the anisotropy is below the noise level. One sign of this is the seemingly random and incoherent orientations of anisotropy ellipses.

In both Unayzah-C and Unayzah-A reservoirs the highest anisotropy intensity is located along the relatively steeper western flank of the field structure, which is also in

agreement with curvature and coherence attributes which also show maximum fracturing along the steep western flank of the field structure. Otherwise, there is no correlation between AVOA, curvature and coherence results. I see that the general strike of the anisotropy ellipses is discordant to the main structural trend.

The ellipticity values greater than 1 is arbitrary and it may change with reservoir lithology and heterogeneity, depth, seismic data quality. There are two other possible explanations — besides weakness of anisotropy — for the low correlation between ellipticity and natural fractures:

1. Granulation.
2. Reservoir heterogeneity.

Granulation seams and deformation bands are far more common in clastic reservoirs than open fluid conductive fracture zones. These features are filled with sand and clay gouge and have a lower permeability than the matrix. As such they do not impart significant amplitude or velocity anisotropy.

Unayzah-C reservoir is an extremely heterogeneous glacial deposit with some shear bands associated with glacial advance and retreat. Unayzah-A reservoir is a cross bedded eolian sandstone. The heterogeneity and cross bedding may adversely affect the seismic anisotropy. For future research work, it is suggested to carefully process the input data using the approach by Burnstad and Keho (2011) to eliminate to some extent the stratigraphic effects and hence enhance the results of the AVOA method (Sayers, 2007).

REFERENCES

[1] Aki, K.; and Richards, P.G.;, Quantitative seismology: Theory and methods, CA: W. H. Freeman and Co, 1980.

[2] Alford, R.M.;, "Shear data in the presence of azimuthal anisotropy," 56th Annual International Meeting of the Society Exploration Geophysicists, Expanded Abstracts, pp. 476- 479, 1986.

[3] Alqahtani, F.M.; and Al-Shuhail, A.A.;, "Imaging subtle faults using azimuthal coherence attribute: a case study from Central Saudi Arabia," *GeoArabia*, vol.17, no.4, pp. 43- 54, 2013.

[4] Al-Dajani, A.A.;, "Fracture detection and characterization for the Jurassic carbonate reservoirs using 3-D P-wave pre-stack seismic data in Saudi Arabia," 8th Middle East Geosciences Conference and Exhibition, GEO2008.

[5] Al-Hawas, K.; Ameen, M.; Wahab, M.; Nebrija, E.; and MacBeth, C.;, "Delineation of fracture anisotropy signatures in Wudayhi Field by azimuthal seismic data," *The Leading Edge*, vol.22, no.12, pp. 1202- 1211, Dec 2003.

[6] Al-Marzoug, A.M.; Neves, F.A.; Kim, J.J.; and Nebrija, E.L.;, "P-wave anisotropy from azimuthal AVO and velocity estimates using 3D seismic data from Saudi Arabia," *Geophysics*, vol.71, no.2, pp. E7- E11, Mar-Apr 2006.

[7] Al-Shuhail, A.A.;, "Seismic characterization of fracture orientation in the Austin Chalk using azimuthal P-wave AVO," Ph.D. dissertation, Texas A&M University, 1998.

[8] Al-Shuhail, A.A.;, "Estimation of fracture porosity using azimuthal P-wave AVO: a case study in the Austin Chalk, Gonzales County, Texas," *Journal of Seismic Exploration*, vol.12, pp. 315- 326, 2004.

[9] Al-Shuhail, A.A.;, "Fracture porosity inversion from P-wave AVOA data along 2-D seismic lines: an example from the Austin Chalk of southeast Texas," *Geophysics*, vol.72, no.1, pp. B1- B7, Jan-Feb 2007.

[10] Balhareth, H.;, "Fracture detection using Azimuthal P-wave Amplitude Variation with Offset (AVOA) in a Carbonate Reservoir, Khurais Field, Saudi Arabia," M.Si. Thesis, King Fahd University of Petroleum & Minerals, 2009.

[11] Burnstad, R.M.; and Keho, T.H.;, "Target-oriented stratigraphic processing for AVZ analysis," *The Leading Edge*, vol.30, no.7, pp. 740- 749, Jul 2011.

[12] Cary, P.W.;, "Common offset vector gathers: an alternative to cross-spreads for wide-azimuth 3D surveys," 69th Annual International Meeting of the Society Exploration Geophysicists, Expanded Abstracts, pp. 1496- 1499, 1999.

[13] Crampin, S.; Evans, R.; Üçer, B.; Doyle, M.; Davis, J.P.; Yegorkina, G.V.; and Miller, A.;, "Observations of dilatancy-induced polarization anomalies and earthquake prediction," *Nature*, vol.286, pp. 874- 877, 1980.

[14] Grechka, V.; and Tsvankin, I.;, "3-D description of normal moveout in anisotropic inhomogeneous media," *Geophysics*, vol.63, no.3, pp. 1079- 1092, May-Jun 1998.

[15] Gray, D.; and Head, K.;, "Fracture detection in Manderson Field: A 3-D AVAZ case history," *The Leading Edge*, vol.19, no.11, pp. 1214- 1221, Nov 2000.

[16] Hall, S.A.; Kendall, J.M.; and Barkved, O.I.;, "Fractured reservoir characterization using P-wave AVOA analysis of 3D OBC data," *The Leading Edge*, vol.21, no.8, pp. 777- 781, Aug 2002.

[17] Jenner, E.;, "Azimuthal anisotropy of 3-D compressional wave seismic data, Weyburn field, Saskatchewan, Canada," Ph.D. dissertation, Colorado School of Mines University, 2001.

[18] Jenner, E.;, "Azimuthal AVO: Methodology and data examples," *The Leading Edge*, vol.21, no.8, pp. 781- 786, Aug 2002.

[19] Lefeuvre, F.; Nicoletis, L.; Ansel, V.; and Cliet, C.;, "Detection and measure of the shear-wave birefringence from vertical seismic data: Theory and applications," *Geophysics*, vol.57, no.11, pp. 1463- 1481, Nov 1992.

[20] Liu, E.; Chapman, M.; Varela, I.; Li, X.; Queen, J.H.; and Lynn, H.;, "Velocity and attenuation anisotropy: Implication of seismic fracture characterizations," *The Leading Edge*, vol.26, no.9, pp. 1170- 1174, Sep 2007.

[21] Liu, E.; Zelewski, G.; Lu, C-P.; Reilly, J.M.; and Shevchek, Z.J.;, "Mitigation of overburden effects in fracture prediction using azimuthal AVO," *The Leading Edge*, vol.30, no.7, pp. 751- 756, Jul 2011.

[22] Lynn, H.B.; and Thomsen, L.;, "Reflection shear-wave data collected near the principal axis of azimuthal anisotropy," *Geophysics*, vol.55, no.2, pp. 147- 156, Feb 1990.

[23] Melvin, J.; and Sprague, R.;, "Advances in Arabian stratigraphy: Origin and stratigraphic architecture of glaciogenic sediments in Permian-Carboniferous lower Unayzah sandstones, Eastern Central Saudi Arabia," *GeoArabia*, vol.11, pp. 105- 152, 2006.

[24] Melvin, J.; Sprague, R.; and Heine, C.;, "From bergs to ergs: The late Paleozoic Gondwanan glaciation and its aftermath in Saudi Arabia," *Geological Society of America Special Paper*, vol.468, pp. 37- 80, 2010.

[25] Melvin, J.; and Norton, A.;, "Advances in Arabian stratigraphy: Comparative studies of glaciogenic Juwayl and lower Unayzah strata (Carboniferous-Permian) of Saudi Arabia," *GeoArabia*, vol.18, no.1, pp. 97- 134, 2013.

[26] Neves, F.; Al-Marzoug, A.; Kim, J.; and Nebrija, E.;, "Fracture characterization of deep tight gas sands using azimuthal velocity and AVO seismic data in Saudi Arabia," *The Leading Edge*, vol.22, no.5, pp. 469- 475, May 2003.

[27] Ostrander, W.J.;, "Plane-wave reflection coefficients for gas sands at non normal angles of incidence," *Geophysics*, vol.49, no.10, pp. 1637- 1648, Oct 1984.

[28] Pecholcs, P.; Al-Saad, R.; Al-Sannaa, M.; Quigley, J.; Bagaini, C.; Zarkhidze, A.; May, R.; Guellili, M.; Sianaj, S.; and Membrouk, M.;, "A broadband full azimuth land seismic case study from Saudi Arabia using a 100,000 channel recording system at 6 terabytes per day: acquisition and processing lessons learned," Annual International Meeting of the Society Exploration Geophysicists, Expanded Abstracts, Las Vegas, 2012.

[29] Rüger, A.; and Tsvankin, I.;, "Using AVO for fracture detection: Analytic basis and practical solutions," *The Leading Edge*, vol.16, no.10, pp. 1429- 1434, Oct 1997.

[30] Sayers, C.;, "Introduction to this special section: Fractures," *The Leading Edge*, vol.26, no.9, pp. 1102- 1105, Sep 2007.

[31] Sen, M.K.; Lane, F.D.; and Foster, D.J.;, "Anomalous reflection amplitudes from fractured reservoirs—Failure of AVOA?," *The Leading Edge*, vol.26, no.9, pp. 1148- 1152, Sep 2007.

[32] Sheriff, R.E.;, Encyclopedic Dictionary of Applied Geophysics. Tulsa: SEG Publication, 2002.

[33] Shuey, R.T.;, "A simplification of the Zoeppritz equations," *Geophysics*, vol.50, no.4, pp. 609- 614, Apr 1985.

[34] Sun, S.Z.; Xiao, X.; Chen, L.; Yang, P.; Yang, H.; and Luo, C.;, "P-wave fracture prediction algorithm using data with limited azimuthal distribution," *The Leading Edge*, vol.31, no.2, pp. 198- 205, Feb 2012.

[35] Thomsen, L.;, "Weak elastic anisotropy," *Geophysics*, vol.51, no.10, pp. 1954- 1966, Oct 1986.

[36] Thomsen, L.; Tsvankin, I.; and Mueller, M.C.;, "Layer-stripping of azimuthal anisotropy from reflection shear-wave data," 65th Annual International Meeting of the Society Exploration Geophysicists, Expanded Abstracts, pp. 289- 292, 1995.

[37] Treadgold, G.; Sicking, C.; Sublette, V.; and Hoover, G.;, "Azimuthal processing for fracture prediction and image improvement," *CSEG Recorder*, vol.33, no.5, pp. 40- 44, May 2008.

[38] Vermeer, G.J.;, 3-D seismic survey design. SEG Publication, 2002.

[39] Wallick, B.; Giroldi, L.; Mustafa, H.; Suleiman, A.; Lowden, D.; Elsadany, K.; Ahmed, M.; and Fainstein, R.;, "A broadband full azimuth land seismic case study from Saudi Arabia: interpretation and inversion lessons learned," Annual International Meeting of the Society Exploration Geophysicists, Expanded Abstracts, Las Vegas, 2012.

[40] Wallick, B.; and Giroldi, L.;, "Interpretation of full-azimuth broadband land data from Saudi Arabia and implications for improved inversion, reservoir characterization and exploration," *Interpretation*, vol.1, no.2, pp. T167- T176, Nov 2013.

[41] Williams, M.; and Jenner, E.;, "Interpreting seismic data in the presence of azimuthal anisotropy; or azimuthal anisotropy in the presence of the seismic interpretation," *The Leading Edge*, vol.21, no.8, pp. 771- 774, Aug 2002.

[42] Zoeppritz, K.;, "On the reflection and propagation of seismic waves," *GottigerNachrichten*, vol.1, pp. 66- 84, 1919.

VITAE

Name:	Ali Hassan Mohammed Al-Gawas
Nationality:	Saudi Arabia
Date of Birth:	November 10, 1983
Email:	algawas.3li@gmail.com
Address:	P.O. Box 13985 Dhahran, 31311 Saudi Arabia
Academic Background:	B.S. in Geophysics, Boise State University, May 2007.
Experience:	Reservoir Geophysicist @ Saudi Aramco Reservoir Characterization Department (July 2010 – Present). Geophysicist @ Saudi Aramco Deferent Tasks within The Exploration Organization as a seismic data processer, field geophysicist in seismic data acquisition, wellsite geologist and training programs such as CEFOGA program with CGG and Exploration Technical Program with Saudi Aramco. (July 2007 – July 2010).